and ameliorates insulin resistance in mice[5–7]. Conversely, adiponectin-deficient mice exhibit insulin resistance and diabetes[8,9]. This insulin-sensitizing effect of adiponectin seems to be mediated by an increase in fatty-acid oxidation through activation of AMP kinase[10,11] and PPAR-α[5,6,12]. Here we report the cloning of complementary DNAs encoding adiponectin receptors 1 and 2 (AdipoR1 and AdipoR2) by expression cloning[14–16]. AdipoR1 is abundantly expressed in skeletal muscle, whereas AdipoR2 is predominantly expressed in the liver. These two adiponectin receptors are predicted to contain seven transmembrane domains, but to be structurally and functionally distinct from G-protein-coupled receptors[17–19]. Expression of AdipoR1/R2 or suppression of AdipoR1/R2 expression by small-interfering RNA[20] supports our conclusion that they serve as receptors for globular and full-length adiponectin, and that they mediate increased AMP kinase[10,11] and PPAR-α ligand activities[12], as well as fatty-acid oxidation and glucose uptake by adiponectin.

Globular adiponectin binds more avidly than full-length adiponectin in C2C12 myocytes and skeletal muscle membranes, but this pattern of binding is reversed in hepatocytes and liver membranes[10] (Supplementary Fig. 1a, b). We attempted to isolate cDNA for adiponectin receptors—which mediate antidiabetic effects—from Ba/F3 cells infected with a library of retrovirally expressed cDNA, derived from human skeletal muscle messenger RNA, by screening for globular adiponectin binding[14].

Infected Ba/F3 cells were incubated with globular adiponectin with a red fluorescent probe and subjected to three rounds of sorting (Fig. 1a, b); the sorted cells were then incubated with globular adiponectin with a green fluorescent probe. As the cells that changed from red to green may have specific binding sites for

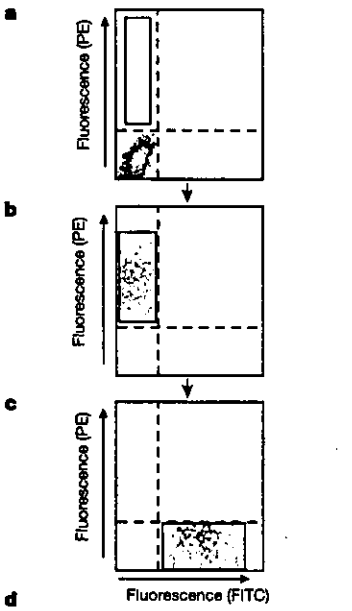


e

Adiponectin receptor

```
                                10        20        30        40        50        60
AdipoR1 (Human)  MSSHKGSVVA QGNGAPASNR EADTVELAEL GPLLEEKGKR VIANPPKAEE EQTCPVPQEE
AdipoR1 (Mouse)  MSSHKGSAGA QGNGAPSGNR EADTVELAEL GPLLEEKGKR AASSPAKAEE DQACPVPQEE
                 ---------- ---------- ---------- ---------- ---------- ----------
                 ---------- ---------- ---------- ---------- ---------- ----------
                                70        80        90       100       110       120
AdipoR1 (Human)  EEEVRVLTLP LQAHHAMEKM EEFVYKVWEG RWRVIPYDVL PDWLKDNDYL LHGHRPPMPS
AdipoR1 (Mouse)  EEEVRVLTLP LQAHHAMEKM EEFVYKVWEG RWRVIPYDVL PDWLKDNDYL LHGHRPPMPS
AdipoR2 (Human)  ---------- ------MEKM EEFVCKVWEG RWRVIPHDVL PDWLKDNDFL LHGHRPPMPS
AdipoR2 (Mouse)  ----MGMSPL LQAHHAMERM EEFVCKVWEG RWRVIPHDVL PDWLKDNDFL LHGHRPPMPS
                               130       140       150       160       170       180
AdipoR1 (Human)  FRACFKSIFR IHTETGNIWT HLLGFVLFLF LGILTMLRPN MYFMAPLQEK VVFGMFFLGA
AdipoR1 (Mouse)  FRACFKSIFR IHTETGNIWT HLLGFVLFLF LGILTMLRPN MYFMAPLQEK VVFGMFFLGA
AdipoR2 (Human)  FRACFKSIFR IHTETGNIWT HLLGCVFFLC LGIFYMFRPN ISFVAPLQEK VVFGLFFLGA
AdipoR2 (Mouse)  FRACFKSIFR IHTETGNIWT HLLGCVFFLC LGIFYMFRPN ISFVAPLQEK VVFGLFFLGA
                               190       200       210       220       230       240
AdipoR1 (Human)  VLCLSFSWLF HTVYCHSEKV SRTFSKLDYS GIALLIMGSF VPWLYYSFYC SPQPRLIYLS
AdipoR1 (Mouse)  VLCLSFSWLF HTVYCHSEKV SRTFSKLDYS GIALLIMGSF VPWLYYSFYC SPQPRLIYLS
AdipoR2 (Human)  ILCLSFSWLF HTVYCHSEGV SRLFSKLDYS GIALLIMGSF VPWLYYSFYC NPQPCFIYLI
AdipoR2 (Mouse)  ILCLSFSWLF HTVYCHSEGV SRLFSKLDYS GIALLIMGSF VPWLYYSFYC NPQPCFIYLI
                               250       260       270       280       290       300
AdipoR1 (Human)  IVCVLGISAI IVAQWDRFAT PKHRQTRAGV FLGLGLSGVV PTMHFTIAEG FVKATTVGQM
AdipoR1 (Mouse)  IVCVLGISAI IVAQWDRFAT PKHRQTRAGV FLGLGLSGVV PTMHFTIAEG FVKATTVGQM
AdipoR2 (Human)  VICVLGIAAI IVSQWDMFAT PQYRGVRAGV FLGLGLSGII PTLHYVISEG FLKAATIGQI
AdipoR2 (Mouse)  VICVLGIAAI IVSQWDMFAT PQYRGVRAGV FVGLGLSGII PTLHYVISEG FLKAATIGQI
                               310       320       330       340       350       360
AdipoR1 (Human)  GWFFLMAVMY ITGAGLYAAR IPERFFPGKF DIWFQSHQIF HVLVVAAAFV HFYGVSNLQE
AdipoR1 (Mouse)  GWFFLMAVMY ITGAGLYAAR IPERFFPGKF DIWFQSHQIF HVLVVAAAFV HFYGVSNLQE
AdipoR2 (Human)  GWLMLMASLY ITGAALYAAR IPERFFPGKC DIWFHSHQLF HIFVVAGAFV HFHGVSNLQE
AdipoR2 (Mouse)  GWLMLMASLY ITGAALYAAR IPERFFPGKC DIWFHSHQLF HIFVVAGAFV HFHGVSNLQE
                               370       380       390       400       410       420
AdipoR1 (Human)  FRYGLEGGCT DDTLL..... .......... .......... .......... ..........
AdipoR1 (Mouse)  FRYGLEGGCT DDSLL..... .......... .......... .......... ..........
AdipoR2 (Human)  FRFMIGGGCS EEDAL..... .......... .......... .......... ..........
AdipoR2 (Mouse)  FRFMIGGGCT EEDAL..... .......... .......... .......... ..........
```

**Figure 1** Expression cloning of adiponectin receptors. **a–c**, Globular adiponectin binding to Ba/F3 cells transfected with a skeletal muscle cDNA library. **a**, Transfected cells were incubated with biotinylated globular adiponectin stained with a red fluorescent probe (phycoerythrin, PE). **b**, Cells before the third sorting. **c**, Cells incubated with globular adiponectin conjugated with fluorescein isothiocyanate (FITC) before the fourth sorting. Rectangles indicate globular adiponectin binding positive cells; the cells in the rectangles were sorted in **a–c**. **d**, Northern blot analysis of AdipoR1 (top panel) and AdipoR2 (bottom panel) mRNA in mouse tissues (lanes: 1, brain; 2, heart; 3, kidney; 4, liver; 5, lung; 6, skeletal muscle; 7, spleen; 8, testis). **e**, Amino acid sequences of human and mouse AdipoR1 and AdipoR2.

globular adiponectin (Fig. 1c), integrated cDNA of these cells was sequenced.

The cDNA analysed encoded a protein that we termed AdipoR1 (Supplementary Fig. 1c). Human and mouse AdipoR1 share 96.8% identity (Supplementary Fig. 1c). There may be two types of adiponectin receptor with distinct binding affinity for globular or full-length adiponectin[10] (Supplementary Fig. 1a, b). Indeed, there was one more open reading frame derived from a gene distinct from AdipoR1 in the human and mouse database[15,16], which we termed AdipoR2. Human and mouse AdipoR2 share 95.2% identity (Supplementary Fig. 1c). Human and mouse AdipoR1 is located at chromosome 1p36.13-q41 and 1 E4, whereas AdipoR2 is located at chromosome 12p13.31 and 6 F1, respectively[15,16].

Northern blotting of mouse (Fig. 1d) or human tissues (Supplementary Fig. 1d) identified a major, single band of 2.0 kilobases (kb) for AdipoR1 with the predicted size[15,16]. AdipoR1 was expressed ubiquitously, with the most abundant expression occurring in skeletal muscle. Northern blotting analysis identified a major 4.0-kb single band for AdipoR2 with the predicted size[15,16]. AdipoR2 was most abundantly expressed in the mouse liver.

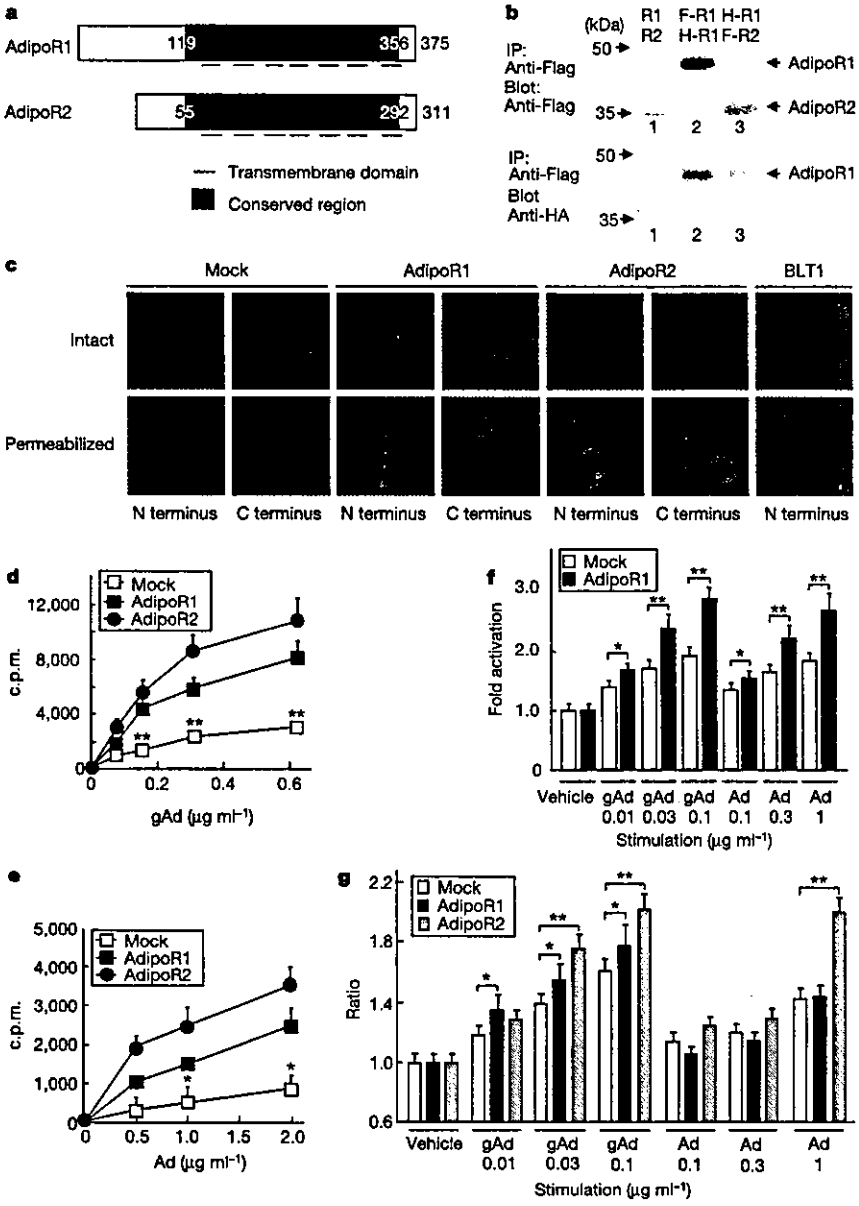


**Figure 2** Localization of AdipoR1 and AdipoR2, and effects of adiponectin receptor expression. **a**, Schematic structure of mouse AdipoR1 and AdipoR2. **b**, Formation of homo- or heteromultimers by human AdipoR1 and AdipoR2. F, Flag tag; H, haemagglutinin tag. **c**, Localization of AdipoR1, AdipoR2 or BLT1 (GPCR, ref. 18) with epitope tags at either end. **d–g**, Binding of $^{125}$I-labelled globular (**d**, gAd) or full-length (**e**, Ad) adiponectin, PPAR-α ligand activity (**f**) and fatty-acid oxidation (**g**) in mouse AdipoR1- or Adipo-R2-transfected C2C12 myocytes after treatment for 7 h with the indicated concentration (μg ml$^{-1}$) of adiponectin. c.p.m., counts per minute. Each bar represents the mean ± s.e.m. ($n = 4$–6). Asterisk, $P < 0.05$; double asterisk, $P < 0.01$; between the two groups indicated, or compared with untreated.

Mouse AdipoR1 encodes a protein of 375 amino acids with the predicted molecular mass of 42.4 kDa, whereas mouse AdipoR2 encodes a protein of 311 amino acids with the predicted molecular mass or 35.4 kDa (Fig. 1e). AdipoR1 and AdipoR2 are structurally highly related—mouse AdipoR1 and AdipoR2 share 66.7% identity (Fig. 1e). AdipoR1 and AdipoR2 were predicted to encode seven transmembrane domain proteins (Fig. 2a). Although there are no other mammalian proteins that share significant sequence homology with AdipoR1 and AdipoR2 in SWISS-PROT, the proteins are conserved from yeast to human especially in the membrane-spanning regions—there are gene products in *Saccharomyces cerevisiae* (accession number Z74744), *Caenorhabditis elegans* (accession number NM_068597) and *Drosophila* (accession number BT001487) that show a marked homology to AdipoR1 (the human protein and these proteins share 29%, 56% and 60% identity, respectively). Notably, the yeast homologue has a principal role in metabolic pathways that regulate lipid metabolism such as fatty-acid oxidation[21]. Although AdipoR1 and AdipoR2 are distantly related to G-protein-coupled receptor (GPCR) families[17–19] in the evolutionary tree (Supplementary Fig. 1e), sequence homology of AdipoR1 and AdipoR2 to the members of GPCR families[17–19] is low.

Both human (Fig. 2b, top panel) and mouse (data not shown) AdipoR1 and AdipoR2 display the predicted molecular mass. We were able to detect AdipoR1 with the epitope tag haemagglutinin (HA) in anti-Flag antibody immunoprecipitates containing Flag-

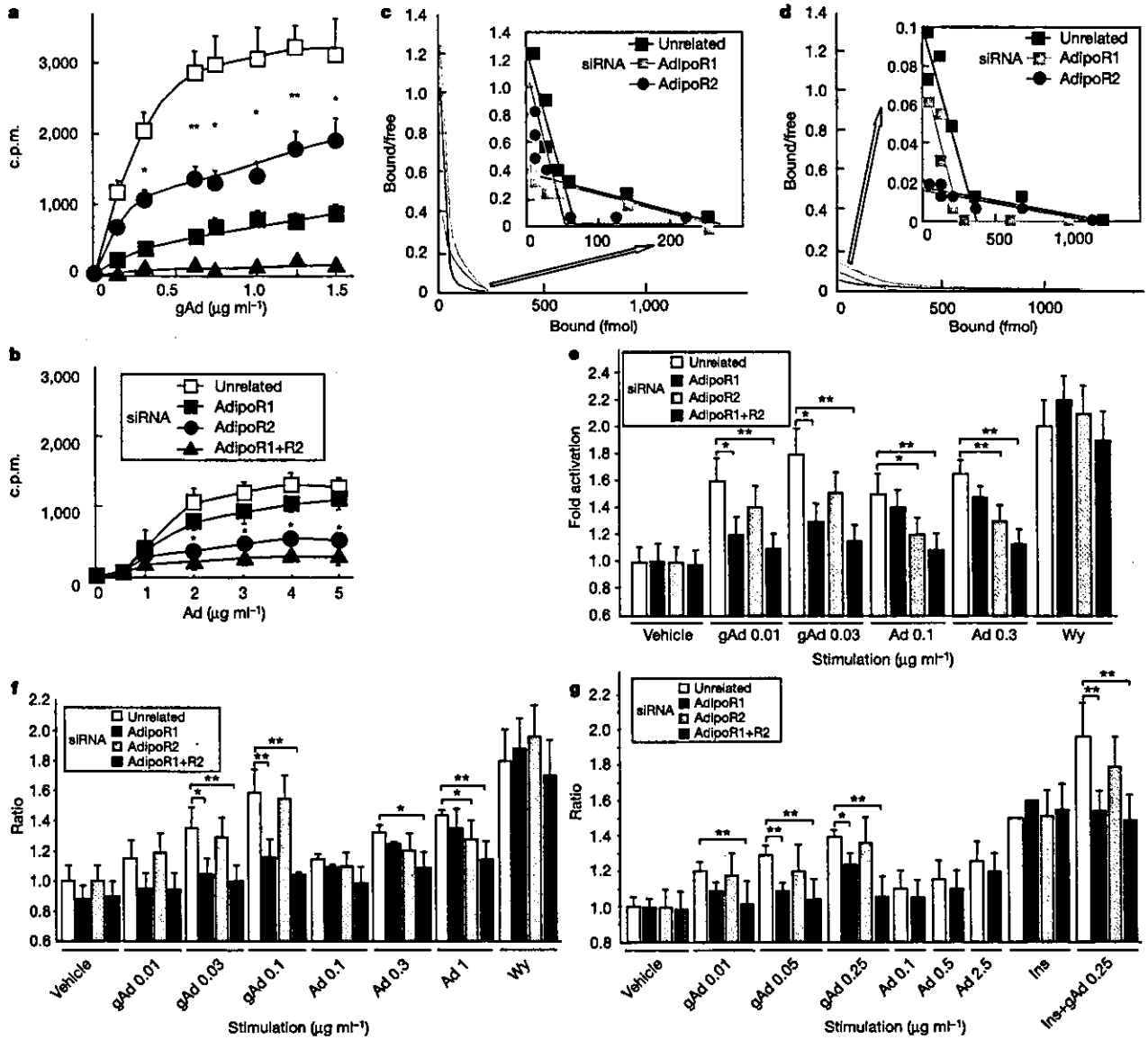


**Figure 3** Effects of suppression of AdipoR1 or AdipoR2 expression by siRNA in mouse C2C12 myocytes. **a–d**, Binding (**a**, **b**) or Scatchard analysis (**c**, **d**) of $^{125}$I-labelled globular (**a**, **c**) or full-length adiponectin (**b**, **d**) to C2C12 myocytes transfected with siRNA duplex. **e–g**, PPAR-α ligand activity (**e**), fatty-acid oxidation (**f**) and glucose uptake (**g**) in C2C12 myocytes transfected with the indicated siRNA duplex. Wy, PPAR-α agonist Wy-14,643. Each bar represents the mean ± standard error ($n = 3$–8). Asterisk, $P < 0.05$; double asterisk, $P < 0.01$; between the two groups indicated, or compared with cells transfected with unrelated siRNA.

tagged AdipoR1 and AdipoR2 (Fig. 2b, bottom panel), suggesting that AdipoR1 and AdipoR2 may be able to form both homo- and heteromultimers.

When the epitope tag was inserted at the amino terminus, we were able to detect AdipoR1 and AdipoR2 at the cell surface and intracellular organelles only when the cells were permeabilized. In contrast, when the epitope tag was inserted at the carboxy terminus we were able to detect AdipoR1 and AdipoR2 at the cell surface without permeabilization (Fig. 2c). These data indicate that AdipoR1 and AdipoR2 are integral membrane proteins—the N terminus was internal and the C terminus was external, which is opposite to the topology of all the reported GPCR families[17–19].

Expression of AdipoR1 or AdipoR2 at the cell surface in 293T cells enhanced the binding of both globular and full-length adiponectin (Supplementary Fig. 2a, b). In 293T cells expressing AdipoR1, globular or full-length adiponectin had little effect on

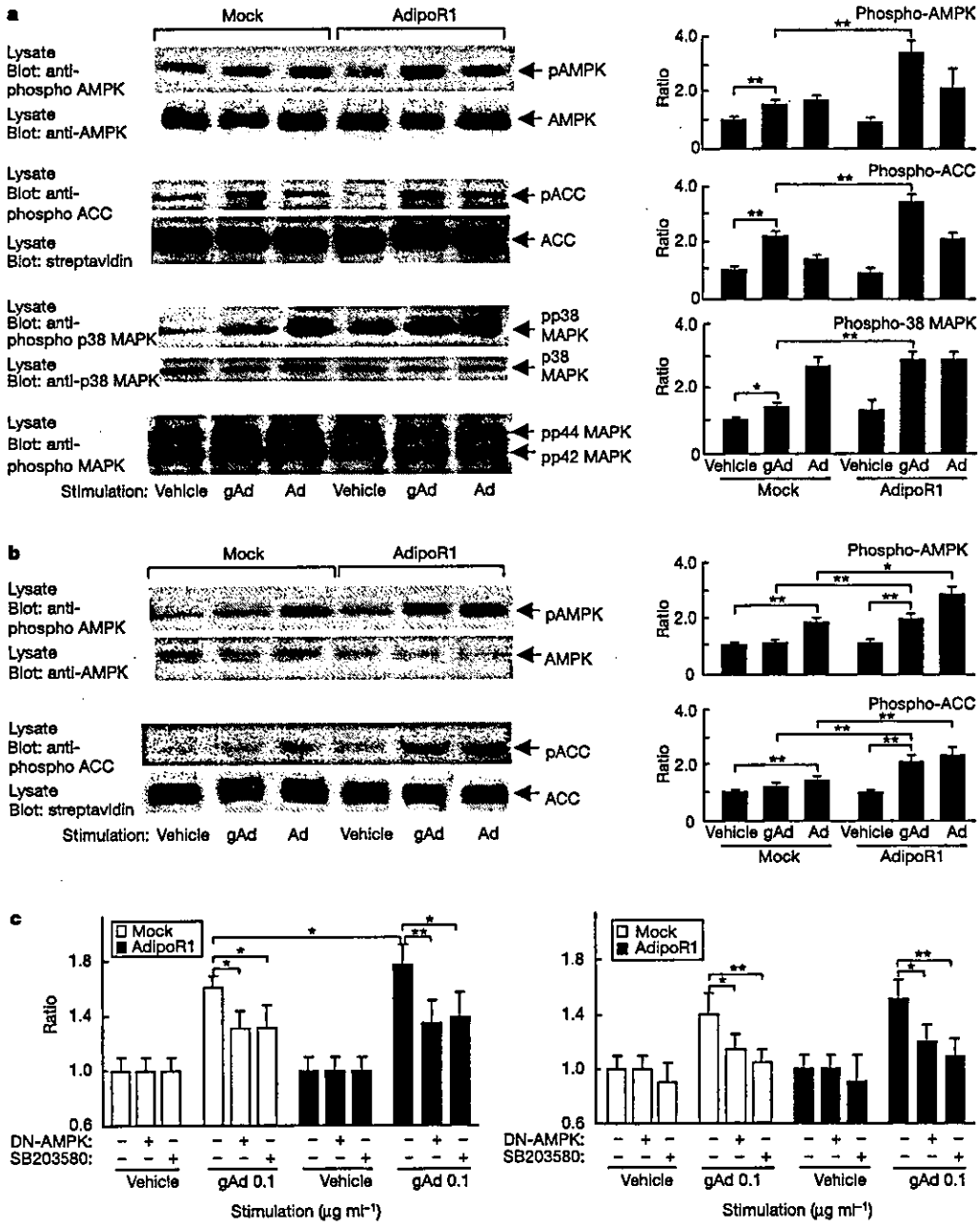


**Figure 4** Effects of expression of AdipoR1 on adiponectin-stimulated intracellular signals and biological effects. **a**, **b**, Phosphorylation and amount of AMPK (first panels), ACC (second panels), p38 MAPK (third panels) and MAPK (fourth panel) incubated with 0.1 μg ml$^{-1}$ globular adiponectin or 1 μg ml$^{-1}$ full-length adiponectin for 10 min in C2C12 myocytes (**a**) or hepatocytes (**b**) transfected with or without AdipoR1. **c**, Fatty-acid oxidation (left panel) and glucose uptake (right panel) in mouse C2C12 myocytes. Each bar represents the mean ± standard error ($n = 3$–5). Asterisk, $P < 0.05$; double asterisk, $P < 0.01$; between the two groups indicated.

cyclic AMP, cyclic GMP and intracellular calcium levels (Supplementary Fig. 2c, d). In contrast, expression of AdipoR1 enhanced increases in PPAR-α ligand activity by both globular and full-length adiponectin (Supplementary Fig. 2e).

Expression of AdipoR1 or AdipoR2 in C2C12 myocytes (Supplementary Fig. 3a, b) enhanced both globular and full-length adiponectin binding (Fig. 2d, e), which were associated with increases in PPAR-α ligand activity (Fig. 2f) and fatty-acid oxidation (Fig. 2g) by both globular and full-length adiponectin. These data indicated that AdipoR1 and AdipoR2 are able to mediate the binding of globular and full-length adiponectin, as well as increases in PPAR-α ligand activity and fatty-acid oxidation by globular and full-length adiponectin.

C2C12 myocytes transfected with unrelated small-interfering (si)RNA[20] bound globular adiponectin more avidly than full-length adiponectin (Fig. 3a, b). Scatchard plot analysis revealed that there are two binding sites for globular adiponectin (Fig. 3c): high-affinity binding sites (dissociation constant ($K_d$) approximately 0.06 $\mu g\,ml^{-1}$, equivalent to 1.14 nM of the globular adiponectin trimer) and intermediate-affinity binding sites ($K_d$ approximately 0.80 $\mu g\,ml^{-1}$, equivalent to 14.4 nM of the globular adiponectin trimer). In contrast, there are intermediate ($K_d$ value approximately 6.7 $\mu g\,ml^{-1}$, equivalent to 49.1 nM of the full-length adiponectin hexamer) and low-affinity binding sites for full-length adiponectin ($K_d$ value approximately 329.3 $\mu g\,ml^{-1}$, equivalent to 2,415 nM of the full-length adiponectin hexamer) (Fig. 3d).

Suppression of AdipoR1 expression with siRNA (Supplementary Fig. 3c) largely reduced globular adiponectin binding (Fig. 3a) but only barely reduced full-length adiponectin binding (Fig. 3b). Scatchard plot analysis revealed that specific suppression of AdipoR1 abrogated high-affinity binding sites but failed to affect intermediate-affinity binding sites for globular adiponectin (Fig. 3c). Moreover, specific suppression of AdipoR1 only partially reduced intermediate binding sites for full-length adiponectin (Fig. 3d), and abrogated low-affinity binding sites for full-length adiponectin (Fig. 3d). In contrast to AdipoR1, suppression of AdipoR2 expression with siRNA (Supplementary Fig. 3d) largely reduced full-length adiponectin binding (Fig. 3b), but modestly reduced globular adiponectin binding (Fig. 3a). Scatchard plot analysis revealed that specific suppression of AdipoR2 barely reduced high-affinity binding sites for globular adiponectin (Fig. 3c), but abrogated intermediate-affinity binding sites (Fig. 3c). Specific suppression of AdipoR2 abrogated intermediate-affinity binding sites for full-length adiponectin (Fig. 3d), but failed to reduce low-affinity binding sites (Fig. 3d). Together, these data suggested that AdipoR1 is a high-affinity receptor for globular adiponectin and also a low-affinity receptor for full-length adiponectin, and that AdioR2 is an intermediate-affinity receptor for full-length and globular adiponectin.

The treatment of either globular or full-length adiponectin for 7 h increased PPAR-α ligand activity (Fig. 3e) and stimulated fatty-acid oxidation (Fig. 3f) and glucose uptake (Fig. 3g) in C2C12 myocytes transfected with unrelated siRNA. Suppression of AdipoR1 expression by specific siRNA (Supplementary Fig. 3c) greatly reduced increases in PPAR-α ligand activity (Fig. 3e), fatty-acid oxidation (Fig. 3f) and glucose uptake (Fig. 3g) by globular adiponectin. In contrast, the suppression of AdipoR1 expression failed to significantly reduce these effects by full-length adiponectin (Fig. 3e–g). Suppression of AdipoR2 expression by specific siRNA (Supplementary Fig. 3d) partially reduced increases in PPAR-α ligand activity (Fig. 3e) and fatty-acid oxidation (Fig. 3f) by full-length adiponectin, but not by globular adiponectin.

Suppression of both AdipoR1 and AdipoR2 expression in combination by siRNA in C2C12 myocytes (Supplementary Fig. 3c, d) almost abolished globular adiponectin binding (Fig. 3a) and largely abolished full-length adiponectin binding (Fig. 3b), and at the same time almost abolished the increased PPAR-α ligand activity (Fig. 3e), fatty-acid oxidation (Fig. 3f) and glucose uptake (Fig. 3g) by globular or full-length adiponectin.

Mock-transfected hepatocytes specifically bound full-length adiponectin (Supplementary Fig. 3f) but not globular adiponectin (Supplementary Fig. 3e). Expression of AdipoR1 or AdipoR2 alone or in combination made it possible for globular adiponectin to bind to hepatocytes (Supplementary Fig. 3e) and further increased full-length adiponectin binding to hepatocytes (Supplementary Fig. 3f), both of which were associated with increases in PPAR-α ligand activity by globular and full-length adiponectin (Supplementary Fig. 3g). Conversely, suppression of AdipoR2 expression by siRNA in hepatocytes significantly reduced full-length adiponectin binding (Supplementary Fig. 3h) as well as increases in PPAR-α ligand activity by full-length adiponectin (Supplementary Fig. 3i).

In mock-transfected C2C12 myocytes both globular and full-length adiponectin increased the amount of phosphorylation of AMP kinase (AMPK), acetyl coenzyme A carboxylase (ACC)[10,11] and p38 mitogen-activated protein kinase (MAPK)[22–24], but not other protein kinases such as MAPK (Fig. 4a). Expression of AdipoR1 in C2C12 myocytes was associated with increased phosphorylation of AMPK, ACC and p38 MAPK on stimulation with globular adiponectin (Fig. 4a), suggesting that AdipoR1 can mediate globular adiponectin-stimulated AMPK[10,11] and p38 MAPK activation[22–24] (Fig. 4a).

In mock-transfected hepatocytes, full-length but not globular adiponectin stimulated AMPK activation and ACC phosphorylation (Fig. 4b). Expression of AdipoR1 in hepatocytes was associated with increases in AMPK and ACC phosphorylation on stimulation with both globular and full-length adiponectin (Fig. 4b), suggesting that AdipoR1 can mediate globular and full-length adiponectin-stimulated AMPK and ACC phosphorylation.

In mock-transfected C2C12 myocytes, globular adiponectin-stimulated fatty-acid oxidation and glucose uptake were partially inhibited by dominant negative (DN)-AMPK or SB203580, a specific inhibitor of p38 MAPK[22–24] (Fig. 4c). Expression of AdipoR1 in C2C12 myocytes further increased fatty-acid oxidation and glucose uptake on stimulation with globular adiponectin; these effects were also inhibited partially by DN-AMPK or SB203580 (Fig. 4c). Thus, the stimulation of fatty-acid oxidation and glucose uptake by globular adiponectin through AdipoR1 seemed to be dependent on both AMPK and p38 MAPK pathways in C2C12 myocytes.

In this study we have isolated cDNA encoding the adiponectin receptors AdipoR1 and AdipoR2. Expression of these receptors or their suppression supports our conclusion that they serve as receptors for globular and full-length adiponectin, and that they mediate increased AMPK, PPAR-α ligand activity, the fatty-acid oxidation and glucose uptake by adiponectin.

Scatchard plot analyses showed that AdipoR1 is a high-affinity receptor for globular adiponectin but a very low-affinity receptor for full-length adiponectin, and that AdipoR2 is an intermediate affinity receptor for globular and full-length adiponectin. In this respect, fatty-acid oxidation mediated through AdipoR1 was highly sensitive to globular adiponectin (half-maximal effective dose ($ED_{50}$) approximately 0.03 $\mu g\,ml^{-1}$, equivalent to 0.54 nM of the globular adiponectin trimer) but was resistant to full-length adiponectin. Fatty-acid oxidation mediated thorough AdipoR2 was intermediately sensitive to globular or full-length adiponectin ($ED_{50}$ approximately 0.85 $\mu g\,ml^{-1}$, equivalent to 6.23 nM of the full-length adiponectin hexamer). Thus, there was a good correlation between binding affinity (Fig. 3c, d) and adiponectin sensitivity (Fig. 2g), and the $ED_{50}$ corresponded to 13–50% of the $K_d$ on a molar basis.

Interactions between adiponectin and AdipoR1 increased PPAR-α, AMPK and p38 MAPK activation. PPAR-α activation is supposedly involved in adiponectin-stimulated fatty-acid oxidation, but

not glucose uptake. AMPK or p38 MAPK activation may be involved in adiponectin-stimulated fatty-acid oxidation and glucose uptake, as both DN-AMPK and SB203580 partially inhibited adiponectin-stimulated fatty-acid oxidation and glucose uptake in an AdipoR1 expression-dependent fashion. p38 MAPK has been reported to activate PPAR-α through increased phosphorylation of PPAR-α[22] and increased co-activation specifically by PGC-1 (refs 22, 23), thereby stimulating fatty-acid oxidation. p38 MAPK has also been reported to stimulate glucose transport by means of increased MEF2 transcriptional activity through an increase of PGC-1 phosphorylation and activation[24], but not through PPAR-α. However, because the extent of AMPK or p38 MAPK activation by globular or full-length adiponectin cannot fully explain the extent of their biological effects, other signalling pathways also seem to be involved. Finally, identification of the 'missing link' between adiponectin receptors and adiponectin-activated protein kinases is an important next step towards our understanding of the actions of adiponectin.

AdipoR1 and AdipoR2 are predicted to contain seven transmembrane domains, but are structurally, topologically and functionally distinct from GPCRs. They do not seem to be coupled with G protein, but activate unique sets of signalling molecules such as PPAR-α, AMPK and p38 MAPK. Thus, adiponectin receptors may comprise a new receptor family. AdipoR1 and AdipoR2 encode receptors for globular and full-length adiponectin that mediate antidiabetic metabolic effects. Molecular cloning of AdipoR1 and AdipoR2 should facilitate the understanding of molecular mechanisms of adiponectin actions and obesity-linked diseases, such as diabetes and atherosclerosis, and the designing of new antidiabetic and anti-atherogenic drugs with AdipoR1 and AdipoR2 as molecular targets. □

## Methods

### FACS analysis and sequencing of integrated retroviruses

$10^7$ Plat-E packaging cells[25] were transiently transfected with 10 μg human skeletal muscle cDNA library (Clontech) using Lipofectamine Plus (Life Technologies). Ba/F3 cells were infected with 1/20-diluted supernatants corresponding to an estimated multiplicity of infection of 0.3 (ref. 14). For selection, we performed fluorescence-activated cell sorting (FACS) analysis[14].

### Quantitative analysis of AdipoR1/R2 transcripts

For quantification of adiponectin receptor mRNAs we used the real-time polymerase chain reaction method and northern blot[10,18] using cDNA probes corresponding to the *PstI–BstXI*, *BamHI–PstI*, or *EcoRV–Not I* fragment of human AdipoR1, mouse AdipoR1 or human and mouse AdipoR2 cDNA, respectively. The primer sets and the probes for mouse AdipoR1/R2 and human AdipoR1/R2 were as follows: mouse AdipoR1 forward primer ACGTTGGAGAGTCATCCCGTAT, reverse primer CTCTGTGTGGATGCGGAAGAT and the probe CCTGCTACATGGCCACAGACCACCT with a minor groove binder; mouse AdipoR2 forward primer TCCCAGGAAGATGAAGGGTTTAT, reverse primer TTCCATTCGTTCGATAGCATGA and the probe ATGTCCCCGCTCCTACAGGCCC with a minor groove binder; human AdipoR1 forward primer TTCTTCCTCATGGCTGTGATGT, reverse primer AAGAAGCGCTCAGGAATTCG and the probe TCACTGGAGCTGGCCTTTATGCTGC with a minor groove binder; human AdipoR2 forward primer ATAGGGCAGATAGGCTGGTTGA, reverse primer GGATCCGGGCAGCATACA and the probe CTGATGGCCAGCCTCTACATCACAGGA with a minor groove binder.

### Recombinant and purification of circulating adiponectin

Bacterially expressed murine full-length adiponectin and globular adiponectin were generated[10], and circulating adiponectin was purified[4,7]. Immunoblot analysis after cross-linking using BS$^3$ indicated that recombinant full-length or circulating adiponectin forms monomers, trimers, hexamers and species of high molecular mass (Supplementary Fig. 4g), and that recombinant globular adiponectin exists as both a monomer and trimer[10]. No significant differences were observed between recombinant full-length adiponectin and circulating adiponectin in the binding to AdipoR1 and AdipoR2 in C2C12 myocytes (Fig. 3b; see also Supplementary Fig. 4i) and in the biological activity such as stimulation of p38 MAPK phosphorylation (Supplementary Fig. 4h).

### Expression in mammalian cells and characterization

The AdipoR1 or AdipoR2 expression vector was constructed by ligating into the *EcoRV–NotI* site of pCXN2 (ref. 26). DNA transfection was performed by lipofection using Lipofectamine Plus (Life Technologies). The cellular location of AdipoR1 or AdipoR2 was evaluated by confocal fluorescence microscopy using 293T cells. Intracellular $Ca^{2+}$ concentration and cAMP and cGMP contents[18], phosphorylation and amount of AMPK, ACC[10], p38 MAPK and MAPK[22–24], PPAR-α ligand activity[12], [$^{14}$C]$CO_2$ production from [1-$^{14}$C]palmitic acid, and glucose uptake[6,10] were determined.

### Binding assay

Recombinant globular or full-length adiponectin was biotinylated with NHS-LC-biotin (Pierce) (Supplementary Fig. 1a, b). Synthetic adiponectin was labelled with $^{125}$I at Tyr by IODO beads (Pierce) in the presence of Na[$^{125}$I] (2,000 Ci mmol$^{-1}$, Amersham Pharmacia Biotech) according to the manufacturer's protocol (Figs 2 and 3; see also Supplementary Figs 2–4). Cells were seeded at a density of $4.1 \times 10^4$ cells per well. After an overnight culture, the cells were incubated at 4 °C for 1 h with binding buffer (ice-cold phosphate-buffered saline (PBS), 0.1% bovine serum albumin) containing designated concentrations of $^{125}$I-labelled adiponectin (5,000 counts per min per ng protein) plus unlabelled competitors. The binding equilibrium was found to be established when the binding assay was conducted at 4 °C after 1 h. The cells were then washed three times with ice-cold PBS, lysed in 0.1 M NaOH, 0.1% SDS, and the cell-bound radioactivity was determined using a γ-counter[10,18]. Nonspecific binding was determined using a 200-fold excess of unlabelled adiponectin. Specific binding was calculated by subtracting nonspecific binding from the total binding. The values presented in this work represent an average of triplicate determinations of 3–10 experiments. Because of high homology between adiponectin and C1q, we studied C1q binding and found that C1q did not bind to AdipoR1 or AdipoR2 in C2C12 myocytes (data not shown).

### RNA interference

Two pairs of siRNAs were chemically synthesized, annealed and transfected into 60–70% confluent C2C12 myocytes, hepatocytes or human aortic endothelial cells using Lipofectamine Plus (Life Technologies)[20]. The sequences of the sense siRNAs are as follows: mouse AdipoR1, GAGACUGGCAACAUCUGGACATT; mouse AdipoR2, GCUUAGAGACACCUGUUUGUUTT; human AdipoR1, GGACAACGACUAUCUGCUACATT; human AdipoR2, GGAGUUUCGUUUCAUGAUCGGTT. Forty-eight hours after transfection, the cells were lysed.

### Predicted structure of AdipoR1 and AdipoR2

Hydropathy plots of the adiponectin receptor proteins were conducted using the hydrophobicity indices of Kyte and Doolittle[27]. We examined whether AdipoR1 and AdipoR2 have homology to any other class of GPCR by the method described at http://cbrg.inf.ethz.ch/Server/AllAll.html.

Received 31 December 2002; accepted 1 May 2003; doi:10.1038/nature01705.


1. Scherer, P. E., Williams, S., Fogliano, M., Baldini, G. & Lodish, H. F. A novel serum protein similar to C1q, produced exclusively in adipocytes. *J. Biol. Chem.* 270, 26746–26749 (1995).
2. Hu, E., Liang, P. & Spiegelman, B. M. AdipoQ is a novel adipose-specific gene dysregulated in obesity. *J. Biol. Chem.* 271, 10697–10703 (1996).
3. Maeda, K. *et al.* cDNA cloning and expression of a novel adipose specific collagen-like factor, apM1 (AdiPose Most abundant Gene transcript 1). *Biochem. Biophys. Res. Commun.* 221, 286–296 (1996).
4. Nakano, Y., Tobe, T., Choi-Miura, N. H., Mazda, T. & Tomita, M. Isolation and characterization of GBP28, a novel gelatin-binding protein purified from human plasma. *J. Biochem. (Tokyo)* 120, 803–812 (1996).
5. Fruebis, J. *et al.* Proteolytic cleavage product of 30-kDa adipocyte complement-related protein increases fatty acid oxidation in muscle and causes weight loss in mice. *Proc. Natl Acad. Sci. USA* 98, 2005–2010 (2001).
6. Yamauchi, T. *et al.* The fat-derived hormone adiponectin reverses insulin resistance associated with both lipoatrophy and obesity. *Nature Med.* 7, 941–946 (2001).
7. Berg, A. H., Combs, T. P., Du, X., Brownlee, M. & Scherer, P. E. The adipocyte-secreted protein Acrp30 enhances hepatic insulin action. *Nature Med.* 7, 947–953 (2001).
8. Kubota, N. *et al.* Disruption of adiponectin causes insulin resistance and neointimal formation. *J. Biol. Chem.* 277, 25863–25866 (2002).
9. Maeda, N. *et al.* Diet-induced insulin resistance in mice lacking adiponectin/ACRP30. *Nature Med.* 8, 731–737 (2002).
10. Yamauchi, T. *et al.* Adiponectin stimulates glucose utilization and fatty-acid oxidation by activating AMP-activated protein kinase. *Nature Med.* 8, 1288–1295 (2002).
11. Tomas, E. *et al.* Enhanced muscle fat oxidation and glucose transport by ACRP30 globular domain: acetyl-CoA carboxylase inhibition and AMP-activated protein kinase activation. *Proc. Natl Acad. Sci. USA* 99, 16309–16313 (2002).
12. Yamauchi, T. *et al.* Globular adiponectin protected ob/ob mice from diabetes and apoE deficient mice from atherosclerosis. *J. Biol. Chem.* 278, 2461–2468 (2003).
13. Ouchi, N. *et al.* Adipocyte-derived plasma protein, adiponectin, suppresses lipid accumulation and class A scavenger receptor expression in human monocyte-derived macrophages. *Circulation* 103, 1057–1063 (2001).
14. Kitamura, T. *et al.* Efficient screening of retroviral cDNA expression libraries. *Proc. Natl Acad. Sci. USA* 92, 9146–9150 (1995).
15. Waterston, R. H. *et al.* Initial sequencing and comparative analysis of the mouse genome. *Nature* 420, 520–562 (2002).
16. Okazaki, Y. *et al.* Analysis of the mouse transcriptome based on functional annotation of 60,770 full-length cDNAs. *Nature* 420, 563–573 (2002).
17. Wess, J. G-protein-coupled receptors: molecular mechanisms involved in receptor activation and selectivity of G-protein recognition. *FASEB. J.* 11, 346–354 (1997).
18. Yokomizo, T., Izumi, T., Chang, K., Takuwa, Y. & Shimizu, T. A G-protein-coupled receptor for leukotriene B4 that mediates chemotaxis. *Nature* 387, 620–624 (1997).
19. Scheer, A., Fanelli, F., Costa, T., De Benedetti, P. G. & Cotecchia, S. Constitutively active mutants of the alpha 1B-adrenergic receptor: role of highly conserved polar amino acids in receptor activation. *EMBO. J.* 15, 3566–3578 (1996).

20. Miyagishi, M. & Taira, K. U6 promoter-driven siRNAs with four uridine 3' overhangs efficiently suppress targeted gene expression in mammalian cells. *Nature Biotechnol.* 20, 497–500 (2002).
21. Karpichev, I. V., Cornivelli, L. & Small, G. M. Multiple regulatory roles of a novel *Saccharomyces cerevisiae* protein, encoded by YOL002c, in lipid and phosphate metabolism. *J. Biol. Chem.* 277, 19609–19617 (2002).
22. Barger, P. M., Browning, A. C., Garner, A. N. & Kelly, D. P. p38 mitogen-activated protein kinase activates peroxisome proliferator-activated receptor alpha: a potential role in the cardiac metabolic stress response. *J. Biol. Chem.* 276, 44495–44501 (2001).
23. Puigserver, P. *et al.* Cytokine stimulation of energy expenditure through p38 MAP kinase activation of PPARγ coactivator-1. *Mol. Cell* 8, 971–982 (2001).
24. Michael, L. F. *et al.* Restoration of insulin-sensitive glucose transporter (GLUT4) gene expression in muscle cells by the transcriptional coactivator PGC-1. *Proc. Natl Acad. Sci. USA* 98, 3820–3825 (2001).
25. Morita, S., Kojima, T. & Kitamura, T. Plat-E: an efficient and stable system for transient packaging of retroviruses. *Gene Ther.* 7, 1063–1066 (2000).
26. Niwa, H., Yamamura, K. & Miyazaki, J. Efficient selection for high-expression transfectants with a novel eukaryotic vector. *Gene* 108, 193–200 (1991).
27. Kyte, J. & Doolittle, R. F. A simple method for displaying the hydropathic character of a protein. *J. Mol. Biol.* 157, 105–132 (1982).

**Supplementary Information** accompanies the paper on **www.nature.com/nature**.

**Acknowledgements** We are grateful to K. Kirii, A. Itoh, A. Okano, T. Nagano and S. Nakamura for their technical assistance. This work was supported by a Grant-in-Aid for Creative Scientific Research from the Japan Society for the Promotion of Science (to T.K.), and by Health Science Research Grants (Research on Human Genome and Gene Therapy) from the Ministry of Health and Welfare (to T.K.).

**Competing interests statement** The authors declare that they have no competing financial interests.

**Correspondence** and requests for materials should be addressed to T.K. (kadowaki-3im@h.u-tokyo.ac.jp). The GenBank accession numbers for human and mouse AdipoR1 are NM_015999 and BC014875, and for human and mouse AdipoR2 are NM_024551 and XM_132831, respectively.

# Redox regulation of protein tyrosine phosphatase 1B involves a sulphenyl-amide intermediate

**Annette Salmeen*†, Jannik N. Andersen‡, Michael P. Myers‡, Tzu-Ching Meng‡, John A. Hinks*, Nicholas K. Tonks‡ & David Barford***

** Section of Structural Biology, Institute of Cancer Research, Chester Beatty Laboratories, 237 Fulham Road, London SW3 6JB, UK*
*‡ Cold Spring Harbor Laboratory, 1 Bungtown Road, Cold Spring Harbor, New York 11724, USA*
*† Present address: Department of Molecular Pharmacology, Stanford University Medical School, 269 Campus Drive, Stanford University, Stanford, California 94305, USA*

**The second messenger hydrogen peroxide is required for optimal activation of numerous signal transduction pathways, particularly those mediated by protein tyrosine kinases[1–6]. One mechanism by which hydrogen peroxide regulates cellular processes is the transient inhibition of protein tyrosine phosphatases through the reversible oxidization of their catalytic cysteine, which suppresses protein dephosphorylation[7–9]. Here we describe a structural analysis of the redox-dependent regulation of protein tyrosine phosphatase 1B (PTP1B), which is reversibly inhibited by oxidation after cells are stimulated with insulin[8] and epidermal growth factor[9]. The sulphenic acid intermediate produced in response to PTP1B oxidation is rapidly converted into a previously unknown sulphenyl-amide species, in which the sulphur atom of the catalytic cysteine is covalently linked to the main chain nitrogen of an adjacent residue. Oxidation of PTP1B to the sulphenyl-amide form is accompanied by large conformational changes in the catalytic site that inhibit substrate binding. We propose that this unusual protein modification both protects the active-site cysteine residue of PTP1B from irreversible oxidation to sulphonic acid and permits redox regulation of the enzyme by promoting its reversible reduction by thiols.**

Protein tyrosine phosphatases (PTPs) are cysteine-dependent enzymes defined by a PTP signature motif, Cys-$(Xaa)_5$-Arg, at their catalytic site[10]. Owing to its unique environment, the catalytic cysteine has a low $pK_a$, which enhances its function as a nucleophile and renders PTPs susceptible to inactivation by reactive oxygen species such as hydrogen peroxide ($H_2O_2$) and superoxide[11]. To understand the mechanism of the reversibility of PTP1B redox regulation, we integrated X-ray crystallography and mass spectrometry to monitor the changes in the enzyme in response to oxidation. We sought to determine the structure of PTP1B with the catalytic cysteine in the physiologically relevant, reversibly oxidized Cys-SOH (sulphenic acid) state.

After incubating the enzyme with stoichiometric amounts of $H_2O_2$, however, we did not observe formation of sulphenic acid but instead identified an unexpected modification of the catalytic site cysteine residue, which we call a 'sulphenyl-amide' species (Fig. 1a). In addition, when we determined the structure of PTP1B at several stages during a time course of oxidation in response to $H_2O_2$, only the newly identified sulphenyl-amide intermediate was detected, and not the Cys-SOH state (Fig. 1b).

In this time course, almost complete conversion of PTP1B to the sulphenyl-amide species occurred by 2 h, and a similar structure was observed at 5 h. At earlier time points, the electron density maps were consistent with a mixture of both reduced and sulphenyl-amide conformational states. Notably, there was no definitive evidence of a sulphenic acid structure, indicating that the rate of formation of this intermediate is rate limiting in the generation of the sulphenyl-amide species. Alternative conformation refinement with REFMAC[12] accounted for the observed electron density maps, allowing the relative proportions of the reduced and sulphenyl-amide states to be estimated (Supplementary Table 1). After a 16-h incubation, the sulphenyl-amide species was oxidized to a mixture of sulphinic (Cys-$SO_2H$) and sulphonic (Cys-$SO_3H$) acids, and this structure of PTP1B resembled PTP1B-$SO_3H$ generated with pervanadate, a strong oxidizing agent (Supplementary Information).

The oxidation of the catalytic cysteine to the sulphenyl-amide state was accompanied by profound changes in the structure of the active site and inhibition of activity. In reduced PTP1B, the catalytic Cys 215 is at the base of a cleft on the surface of the protein formed by residues of the PTP signature motif (residues 214–222), which create the PTP loop (refs 10, 13 and Fig. 2a). The thiol group of Cys 215 is poised for nucleophilic attack onto the substrate, and the Sγ atom of Cys 215 accepts a hydrogen bond from the side chain of Ser 222. In the sulphenyl-amide state, electron density maps in the region of the PTP loop indicate well-defined continuous density bridging the Sγ-atom of Cys 215 and the main chain nitrogen atom of Ser 216 (Figs 1 and 2b). The sulphenyl-amide species is probably formed by nucleophilic attack of the main chain nitrogen atom of Ser 216 onto the electrophilic sulphur atom of the labile sulphenic acid, with concomitant release of water (Fig. 2c). Notably, $F_o - F_c$ electron density maps show that there are no additional oxygen atoms attached to Sγ of Cys 215 in the sulphenyl-amide species (Fig. 1). This is consistent with the occurrence of a nucleophilic substitution reaction (Fig. 2c).

Formation of the sulphenyl-amide bond, which imposes conformational constraints on the main chain of the PTP loop and disruption of the Cys 215–Ser 222 hydrogen bond, triggers tertiary structural changes in the protein (Fig. 2d). Notably, the PTP loop undergoes a marked change in conformation. Gly 218 shifts by about 7 Å, and the helical conformation of the PTP loop in reduced PTP1B converts to a reverse β-hairpin conformation. The phosphotyrosine (pTyr) loop containing Tyr 46, which defines the depth of

CDKs in late G1 defines a "point of no return" after which Cdc6 synthesis cannot promote DNA replication in yeast. *Genes Dev.* 10, 1516–1531 (1996).
11. Desdouets, C. *et al.* Evidence for a Cdc6p-independent mitotic resetting event involving DNA polymerase α. *EMBO J.* 17, 4139–4146 (1998).
12. Perkins, G., Drury, L. S. & Diffley, J. F. X. Separate $SCF^{CDC4}$ recognition elements target Cdc6 for proteolysis in S phase and mitosis. *EMBO J.* 20, 4836–4845 (2001).
13. Nguyen, V. Q., Co, C. & Li, J. J. Cyclin-dependent kinases prevent DNA re-replication through multiple mechanisms. *Nature* 411, 1068–1073 (2001).
14. Wilmes, G. M. *et al.* Interaction of the S-phase cyclin Clb5 with an 'RXL' docking sequence in the initiator protein Orc6 provides an origin-localized replication control switch. *Genes Dev.* 18, 981–991 (2004).
15. Adams, P. D. *et al.* Retinoblastoma protein contains a C-terminal motif that targets it for phosphorylation by cyclin-cdk complexes. *Mol. Cell. Biol.* 19, 1068–1080 (1999).
16. Chen, J., Saha, P., Kornbluth, S., Dynlacht, B. D. & Dutta, A. Cyclin-binding motifs are essential for the function of p21CIP1. *Mol. Cell. Biol.* 16, 4673–4682 (1996).
17. Drury, L. S., Perkins, G. & Diffley, J. F. X. The cyclin dependent kinase Cdc28p regulates distinct modes of Cdc6p proteolysis during the budding yeast cell cycle. *Curr. Biol.* 10, 231–240 (2000).
18. Pawson, T. Specificity in signal transduction: from phosphotyrosine-SH2 domain interactions to complex cellular systems. *Cell* 116, 191–203 (2004).
19. Elia, A. E. *et al.* The molecular basis for phosphodependent substrate targeting and regulation of Plks by the Polo-box domain. *Cell* 115, 83–95 (2003).
20. Cheng, K. Y., Lowe, E. D., Sinclair, J., Nigg, E. A. & Johnson, L. N. The crystal structure of the human polo-like kinase-1 polo box domain and its phosphopeptide complex. *EMBO J.* 22, 5757–5768 (2003).
21. Durocher, D. *et al.* The molecular basis of FHA domain:phosphopeptide binding specificity and implications for phospho-dependent signaling mechanisms. *Mol. Cell* 6, 1169–1182 (2000).
22. Halford, K. A. *Biochemical Analysis of Yeast Pre-Replicative Complex Assembly.* Thesis, Univ. College London (2003).
23. Li, J. J. & Kelly, T. J. Simian virus 40 DNA replication *in vitro*. *Proc. Natl Acad. Sci. USA* 81, 6973–6977 (1984).

**Supplementary information** accompanies the paper on **www.nature.com/nature.**

**Acknowledgements** We are grateful to members of our laboratory for discussions and for critical reading of the manuscript. We are also grateful to J. Gannon and T. Hunt for discussions as well as human CDK antibodies and $p13^{suc1}$ beads. We thank L. Drury, K. Labib, J. Li, G. Perkins and S. Reed for yeast strains. We also thank N. O'Reilly and the Peptide Synthesis Facility at the London Research Institute. This work was supported by Cancer Research UK and the Human Frontier Science Program Organization. S.M. is supported by JSPS postdoctoral Fellowships for Research Abroad.

**Competing interests statement** The authors declare that they have no competing financial interests.

**Correspondence** and requests for materials should be addressed to J.F.X.D. (john.diffley@cancer.org.uk).

## corrigendum

# Cloning of adiponectin receptors that mediate antidiabetic metabolic effects

**Toshimasa Yamauchi, Junji Kamon, Yusuke Ito, Atsushi Tsuchida, Takehiko Yokomizo, Shunbun Kita, Takuya Sugiyama, Makoto Miyagishi, Kazuo Hara, Masaki Tsunoda, Koji Murakami, Toshiaki Ohteki, Shoko Uchida, Sato Takekawa, Hironori Waki, Nelson H. Tsuno, Yoichi Shibata, Yasuo Terauchi, Philippe Froguel, Kazuyuki Tobe, Shigeo Koyasu, Kazunari Taira, Toshio Kitamura, Takao Shimizu, Ryozo Nagai & Takashi Kadowaki**

*Nature* 423, 762–769 (2003).

In this Letter, Fig. 1 is an illustration of the sorting procedure, rather than an original data set, which we did not explicitly describe. Because the *x*-axis was used for FACS analysis of both FITC- and PE-labelled cells, only the gated population was shown; these data were extracted from the analyses and inserted into a FACS profile. The same file of a single gated population (from Fig. 1c) was mistakenly misused for a part of the plot in Fig. 1b by inserting it into both Fig. 1b and Fig. 1c in the original figure. In order to clear up the confusion surrounding this figure, the original primary data are shown here in the Supplementary Information. The Supplementary Information also includes further details of our cell-sorting procedure, which were not provided in the published protocol. Although these corrections do not affect the conclusions of our paper, we apologize to readers who have been misled by these mistakes. □

**Supplementary information** accompanies the corrigendum on **www.nature.com/nature.**

ANTISENSE AND NUCLEIC ACID DRUG DEVELOPMENT 13:9–17 (2003)


# Stimulatory Effect of an Indirectly Attached RNA Helicase-Recruiting Sequence on the Suppression of Gene Expression by Antisense Oligonucleotides

TAKASHI FUTAMI,*[,1] MAKOTO MIYAGISHI,*[,1] SHIGENORI IWAI,[1] MINORU SEKI,[1] and KAZUNARI TAIRA[1,2]

## ABSTRACT

**Antisense oligonucleotides (ODNs) are powerful tools with which to determine the consequences of the reduced expression of a selected target gene, and they may have important therapeutic applications. Methods for predicting optimum antisense sites are not always effective because various factors, such as RNA-binding proteins, influence the secondary and tertiary structures of RNAs *in vivo*. To overcome this obstacle, we have attempted to engineer an antisense system that can unravel secondary and tertiary RNA structures. To create such an antisense system, we connected the constitutive transport element (CTE), an RNA motif that has the ability to interact with intracellular RNA helicases, to an antisense sequence so that helicase-binding hybrid antisense ODN would be produced in cells. We postulated that this modification would enhance antisense activity *in vivo*, with more frequent hybridization of the antisense ODN with its targeting site. Western blotting analysis demonstrated that a hybrid antisense ODN targeted to the *bcl*-2 gene suppressed the expression of this gene more effectively than did the antisense ODN alone. Our results suggest that the effects of antisense ODNs can be enhanced when their actions are combined with those of RNA helicases.**

## INTRODUCTION

ANTISENSE OLIGONUCLEOTIDES (ODNs) ARE DESIGNED to hybridize to specific mRNA sequences and, thus, to prevent translation (Hélène and Toulmé, 1990). Antisense ODNs can be readily synthesized, are sequence specific, and have the potential to suppress the expression of any mRNA whose sequences are known. They are particularly useful for determining the functions of specific proteins (Al-Alwan et al., 2001; Chu et al., 2001; Deszo et al., 2001), and their potential as therapeutic agents has been demonstrated in animal models and preliminary clinical trials (Cotter et al., 1999; Kushner and Silverman, 2000). Moreover, some ODNs have already been approved as therapeutic agents (de Smet et al., 1999).

Despite recent progress, the selection of effective antisense ODN sequences remains problematic. Secondary and tertiary structural features can block or hide sites in mRNAs that are targeted for hybridization by antisense ODNs, with resultant failure in the suppression of gene expression. It is not always easy to find optimum target sites, which usually include a small single-stranded region. As a result, most active antisense ODNs have been designed empirically, by trial and error, or on the basis of considerations of the thermodynamic or structural prop-

*The first two authors contributed equally to this work.

[1]Department of Chemistry and Biotechnology, School of Engineering, The University of Tokyo, Hongo, Tokyo 113-8656, Japan.

[2]Gene Function Research Laboratory, National Institute of Advanced Industrial Science and Technology (NIAIST), Tsukuba Science City 305-8562, Japan.

erties of the target mRNA. Empirical analyses can require the screening of as many as 50 antisense compounds in a cellular environment (Dean et al., 1994; Monia et al., 1996). Moreover, although the number of oligonucleotide sequences analyzed for selection of potent antisense compounds potentially can be reduced by computer modeling, such protocols cannot always predict the tertiary structural interactions and topologic or steric constraints that are influenced by proteins that interact with RNAs *in vivo* (Ho et al., 1998; Laptev et al., 1994; Patzel et al., 1999; Sczakiel et al., 1993). It is often difficult to overcome such problems in attempts to exploit antisense ODNs, particularly *in vivo*. Indeed, we faced a similar problem in earlier attempts to apply ribozyme technology *in vivo*. To overcome this problem (Warashina et al., 2001), we decided to recruit intracellular RNA helicases, a class of proteins with nonspecific RNA-binding, sliding, and RNA-unwinding activities by exploiting the constitutive transport element (CTE) that interacts with RNA helicases *in vitro* and *in vivo* (Braun et al., 1999; Grüter et al., 1998; Hodge et al., 1999; Kang and Cullen, 1999; Li et al., 1999; Schmitt et al., 1999; Tang et al., 1997; Tang and Wong-Staal, 2000; Westberg et al., 2000). The CTE was discovered as a cytoplasmic transport signal for D-type retroviral RNA (Bray et al., 1994; Zolotukhin et al., 1994), and we demonstrated recently that poly(A) tails also can be used in recruitment of an intracellular RNA helicase (Kawasaki et al., 2002; Kawasaki and Taira, 2002a,b).

We reasoned that it might be useful to design antisense ODNs that could recruit a protein that could, in turn, eliminate any interfering secondary structure and render any site accessible to an antisense ODN. When we used a ribozyme, the transcript consisted of the RNA ribozyme sequence and an RNA [CTE and poly(A) tail] that can interact with an RNA helicase. In contrast, the RNA motif that interacts with an RNA helicase cannot easily be connected directly to an ODN. To create RNA helicase-interacting ODNs, we tried to link an antisense ODN indirectly to an RNA helicase (de la Cruz et al., 1999; Jankowsky et al., 2000; Lee et al., 1993; Wagner et al., 1998). To recruit an RNA helicase to the antisense ODN, we linked CTE to an antisense ODN via a complementary sequence (Fig. 1). We postulated that an RNA helicase, coupled to the antisense ODN, might efficiently guide the antisense ODN to its specific target site by un-

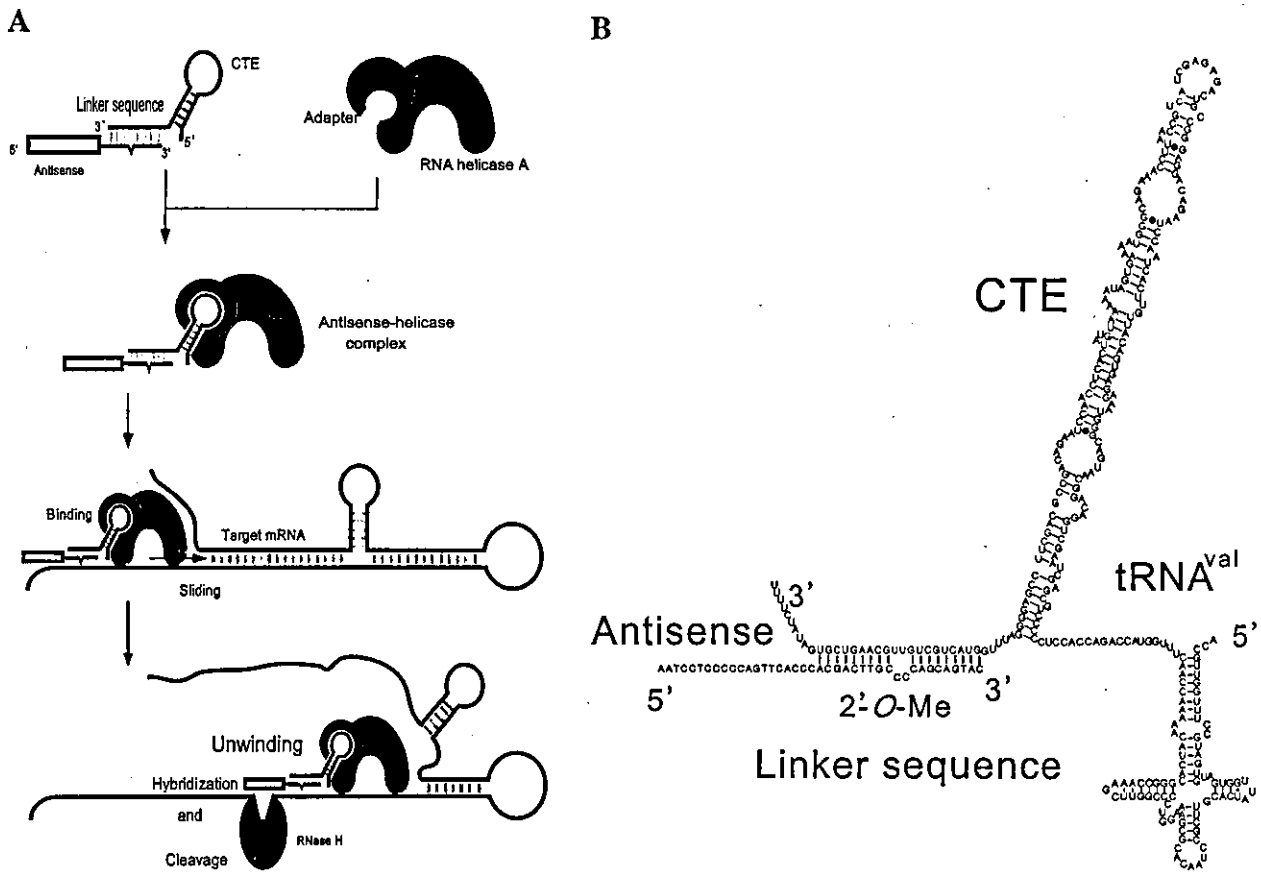


FIG. 1. Schematic representation of the mechanism of action of helicase-binding hybrid antisense ODNs. (A) A CTE-antisense sequence coupled to an RNA helicase can, in theory, hybridize to a hidden target site after elimination of local secondary structure. (B) Specific sequence of the hybrid antisense ODN.

raveling any inhibitory mRNA structures, with subsequent efficient suppression of expression of the targeted mRNA by the antisense ODN.

To examine the validity of our strategy, we targeted an ODN to the transcript of the *bcl*-2 gene, a key gene in the regulation of apoptosis that has been implicated in the chemoresistance of a variety of malignancies via prevention of programmed cell death. Treatment of tumor cells with an antisense ODN targeted to *bcl*-2 mRNA *in vitro* has been shown to suppress expression of the Bcl-2 protein and to induce increased susceptibility to apoptosis (Kamesaki et al., 1993; Miyashita and Reed, 1993; Walton et al., 1993). Inhibition of the action of Bcl-2 should, theoretically, sensitize cells to various cytotoxic chemotherapeutic agents, and, indeed, several partially successful studies in tissue culture and experimental animals have been performed that have led to the initiation of clinical trials.

We demonstrate here that a novel antisense ODN, designed to interact with RNA helicases, can suppress the expression of the *bcl*-2 gene to a significantly greater extent than the parental, unmodified antisense ODN.

## MATERIALS AND METHODS

### *Plasmids*

The CTE-linker fragment was amplified by PCR using the following primer sequence from the CTE-ribozyme (Rz) expression vector (Warashina et al., 2001): forward primer, 5′-ggc ggt acc taa tac gac tca cta tag gga gac cac ctc ccc tgc gag cta ag-3′; reverse primer, 5′-ggc tct aga *gta ctg ctg ttg caa gtc gtc* aaa tcc ctc gga agc tgc gcc tg-3′. Nucleotides in italics indicate the linker sequence that should hybridize with the antisense ODN. The CTE-linker fragment was double-digested with *Kpn*I and *Xba*I and ligated into a $tRNA^{Val}$ expression vector (Warashina et al., 2001). We also generated a CTE expression vector without a linker sequence and the empty (mock) vector without CTE as control vectors.

### *Phosphorothioate-modified oligonucleotides*

Phosphorothioate-modified, 5′-biotinylated ODNs were purchased from ESPEC Oligo Co., Ltd (Tsukuba, Japan). The 20-mer antisense ODN targeted to the coding region of the *bcl*-2 gene and a scrambled-sequence ODN with a similar nucleotide content have been described elsewhere (Ziegler et al., 1997). The sequences were as follows: antisense (AS1) 5′-AAT CCT CCC CCA GTT CAC CC-3′ (ODN2009); scrambled antisense (SC1) 5′-CTC ATT CCT ACC GAC ACC CC-3′—the latter having the same base composition as the former but a randomized sequence. We also generated AS2, namely, 5′-ATC CTC CCC CAG TTC ACC C*acg act tgc* CC*c agc agt ac*-3′, and SC2, namely, 5′-C TCA TTC CTA CCG ACA CCC C*acg act tgc* CC*c agc agt ac*-3′. The ODNs in italics represent linker sequences for hybridization to the CTE-linker sequence. This sequence was 2′-*O*-methylated, and nucleotides to induce formation of a bulge were included (capitalized italic oligonucleotides) to prevent cleavage by RNase H (Walder and Walder, 1988).

### *Cell culture and Western blotting analysis*

HeLa cells were maintained in Dulbecco's modified Eagle's medium (DMEM) that contained 10% fetal bovine serum (FBS), 100 U/ml penicillin G, and 100 $\mu$g/ml streptomycin. Approximately $4 \times 10^4$ cells/well were seeded in 6-well plates and grown in an atmosphere of 5% $CO_2$ in air. Cells were transfected with 0.5 $\mu$g CTE-linker expression vector using the Effectene™ reagent (Qiagen GmbH, Hilden, Germany). At the same time, ODNs (200–400 nM) were introduced using the Oligofectamine™ reagent (Invitrogen, Carlsbad, CA) as recommended by the manufacturer. Cells were harvested 24 hours after transfection and lysed in lysis buffer. After centrifugation of each lysate, equal amounts of protein (20 $\mu$g/lane) were subjected to SDS-PAGE (12.5% polyacrylamide) for 90 minutes at 100 V in glycine buffer (1.92 M glycine and 25 mM Tris, pH 8.3) that contained 1% SDS. Proteins on the gel were transferred electrophoretically to a polyvinylidene difluoride membrane (Millipore Corp., Bedford, MA) in glycine buffer plus 20% methanol for 1 hour at 70 V. The membrane was blocked with 3% skim milk in TBS-T (20 mM Tris, pH 8.2, 137 mM sodium chloride and 0.1% Tween-20). Then, the membrane was incubated with mouse monoclonal antibody (mAb) against human Bcl-2 (1:3000) (Upstate Biotechnology, Lake Placid, NY) and rabbit polyclonal antibodies against actin (1:10,000) (Sigma, St. Louis, MO) in 0.3% skim milk in TBS-T. It was incubated for 1 hour with horseradish peroxidase (HRP)-conjugated antibodies against mouse IgG or against rabbit IgG (1:3,000) (Amersham Biosciences Corp., Piscataway, NJ). Proteins were detected by an enhanced chemiluminescence method (ECL plus) (Amersham Biosciences Corp.). Intensities of bands of immunoreactive proteins were determined using a scanning densitometer using the NIH Image program. The amounts of Bcl-2 protein in cells were normalized by reference to levels of actin.

### *Transfections and confocal immunofluorescence microscopy*

HeLa S3 cells ($4 \times 10^4$/well) were seeded onto glass coverslips in 6-well plates. Cells were transfected with 0.5 $\mu$g DNA using the Effectene reagent. At the same time, ODNs (400 nM) were introduced using the Oligo-

fectamine reagent, as recommended by the manufacturer. Fourteen hours after transfection, the cells were washed twice with phosphate-buffered saline (PBS)(−), fixed for 20 minutes at ambient temperature in PBS(−) that contained 3% (w/v) paraformaldehyde, and permeabilized by incubation with 0.1% (v/v) Triton X-100 in PBS(−) for 30 minutes. After washing with PBS(−), the cells were incubated for 1 hour with Cy2-conjugated streptavidin (1:200) (Amersham Biosciences Corp.) and examined under a confocal microscope (Leica Microsystems, Mannheim, Germany).

## RESULTS AND DISCUSSION

### *Design of CTE-linker expression vector and hybrid antisense molecules*

To create helicase-bound hybrid antisense ODNs that could unravel the secondary and tertiary structure of the target mRNA, we constructed an expression plasmid vector that encoded the CTE-linker under the control of the promoter of a human gene for $tRNA^{Val}$ (note that the $tRNA^{Val}$ motif at the 5′-end has been omitted from Fig. 1A for clarity). The linker sequence adjacent to CTE was designed to hybridize with the complementary linker sequence of an antisense ODN. In choosing the hybridizing sequence, we had to make sure that it exhibited no homology to any known human gene (nor CTE and sense/antisense sequences of *bcl*-2) so that the linker sequence would not suppress the expression of other genes by an antisense effect. A BLASTN search of the NCBI DNA database revealed that the 20-mer linker sequence that we chose was not homologous to any known human gene. Moreover, calculations using RNA-folding algorithms predicted that the linker sequence would not adopt a secondary structure, suggesting that the CTE-containing fragment would successfully hybridize with the antisense ODN via the selected linker sequence.

To avoid the RNase H-mediated degradation of the CTE-containing RNA fragment within the RNA/DNA duplex region, we introduced a bulge into the double-stranded region and 2′-*O*-methylated the linker DNA of the antisense molecule (Furdon et al., 1989).

To achieve high levels of expression of CTE, we used a previously developed RNA polymerase III-mediated expression system in which a hammerhead Rz is embedded within the 3′-terminus of a human gene for $tRNA^{Val}$ (Kawasaki et al., 1998; Kuwabara et al., 1998a,b, 1999; Tanabe et al., 2000). When the transcribed and attached tRNA maintains a cloverleaf-like structure, the transcript should be stabilized, and both should be transported to the cytoplasm (Koseki et al., 1999; Kuwabara et al., 2001a,b). As the CTE sequence from simian type D retrovirus and the adjacent linker sequence were attached to the 3′-end, we expected that they would be expressed at high levels. We also constructed a CTE expression vector without the linker sequence as a control vector, postulating that the resultant transcript, without a linker sequence, would not recognize any RNA helicases.

### *Intracellular localization of antisense ODNs*

The CTE is functionally equivalent to the Rev/RRE sequence of HIV, and presumably, it interacts with cellular export proteins to mediate the nuclear export of unspliced viral RNA. RNA helicase A (RHA) is one of the CTE-binding proteins (Tang et al., 1997), and it is required for CTE activity (Li et al., 1999). RHA shuttles between the nucleus and the cytoplasm, despite its predominant nuclear localization in the steady state (Tang et al., 1997). A bidirectional nuclear transport domain has been identified at the carboxyl-terminus of the protein (Tang et al., 1999).

To determine if the intracellular localization of antisense ODNs might be affected by indirect interactions with the CTE-containing RNA fragment, we cotransfected HeLa S3 cells with a 3′-biotinylated phosphorothioate-modified antisense ODN against *bcl*-2 (to allow staining with Cy2-streptavidin) and either the CTE-linker expression vector or the control CTE expression vector. Then, 24 hours after transfections, we stained the antisense ODN with Cy2-streptavidin. As shown in Figure 2, in all cases examined, antisense ODNs were located predominantly in the nuclei.

In cells that had been transiently cotransfected with the CTE-linker expression vector (Fig. 2c) and ODNs, a small fraction of the antisense ODNs seemed to be localized in the cytoplasm. It appears that as antisense ODNs were not covalently attached to CTE, antisense ODNs that did and did not hybridize to CTE were in equilibrium and that a significant fraction of ODNs was localized in the nucleus without formation of ternary antisense-CTE-RHA complexes.

### *Effects of hybrid antisense ODN on the expression of* bcl-2

Because attachment of the CTE had no significant effect on the intracellular localization of the antisense ODNs, we examined whether the attachment of CTE might influence the intracellular activity of ODNs. Specifically, we quantitated the intracellular activities of antisense and hybrid-antisense ODNs directed against *bcl*-2 by Western blotting analysis. We cotransfected HeLa cells with the antisense or scrambled ODN and the CTE-linker expression vector, the control linkerless CTE expression vector, or the empty vector.

Western blotting analysis revealed that levels of Bcl-2 protein were reduced in cells that had been treated with the *bcl*-2-specific antisense ODN alone at a concentra-

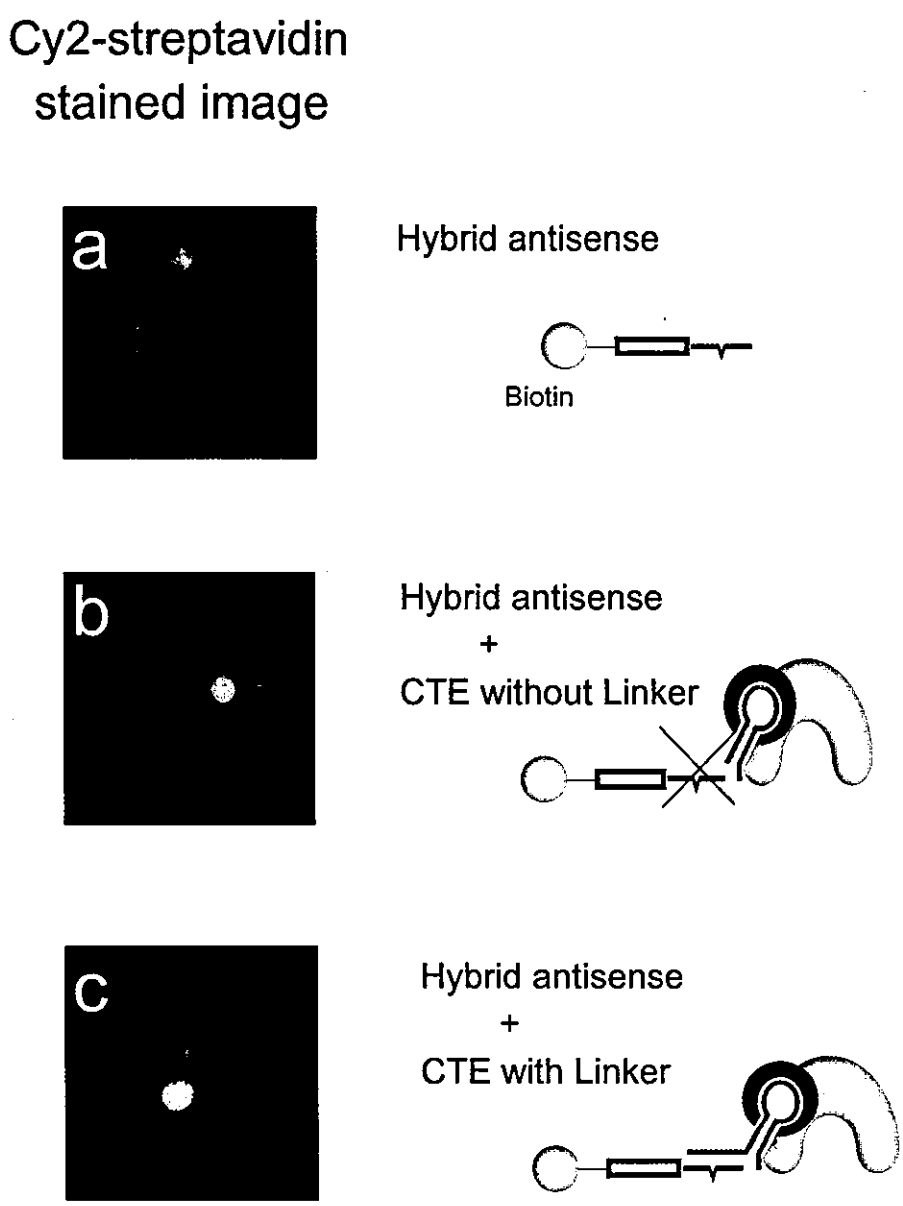


**FIG. 2.** HeLa S3 cells were transfected with the antisense ODN alone (**a**). They were cotransfected with the antisense ODN plus the control linkerless CTE expression vector (**b**). They were cotransfected with the antisense ODN plus the CTE-linker expression vector (**c**). In each case, we used 400 nM 5′-biotinylated phosphorothioate antisense ODN. Fourteen hours after transfection, cells were stained with Cy2-conjugated streptavidin. In a control experiment, we performed transfection with antisense ODN that had not been biotinylated, and we confirmed that no cells were stained with Cy2-conjugated streptavidin (data not shown).

tion of 400 nM (Fig. 3A, lanes 5 and 9), whereas treatment with the scrambled ODN had no effect (Fig. 3A, lanes 2, 3, 6, and 7). Levels of actin were unchanged, indicating that the effect of the antisense ODN was specific to Bcl-2 (Fig. 3A).

Levels of Bcl-2 fell significantly when the CTE-linker expression vector was introduced with the antisense ODN (Fig. 3A, lanes 10 and 11). Importantly, as the addition of the CTE-harboring construct without the linker did not change the antisense effect (Fig. 3A, compared lanes 4 and 5 with lanes 8 and 9), the observed enhancement in the antisense effect in lanes 10 and 11 appeared to have originated from the recruitment of RNA helicase(s). Conclusions from this study in mechanistic terms are somewhat complicated by the fact that free as well as linker-CTE-complexed ODN is located in the nucleus and cytoplasm of cells, as indicated by the results shown in Figure 2. However, as mentioned (Fig. 2c), as a higher level of anti-

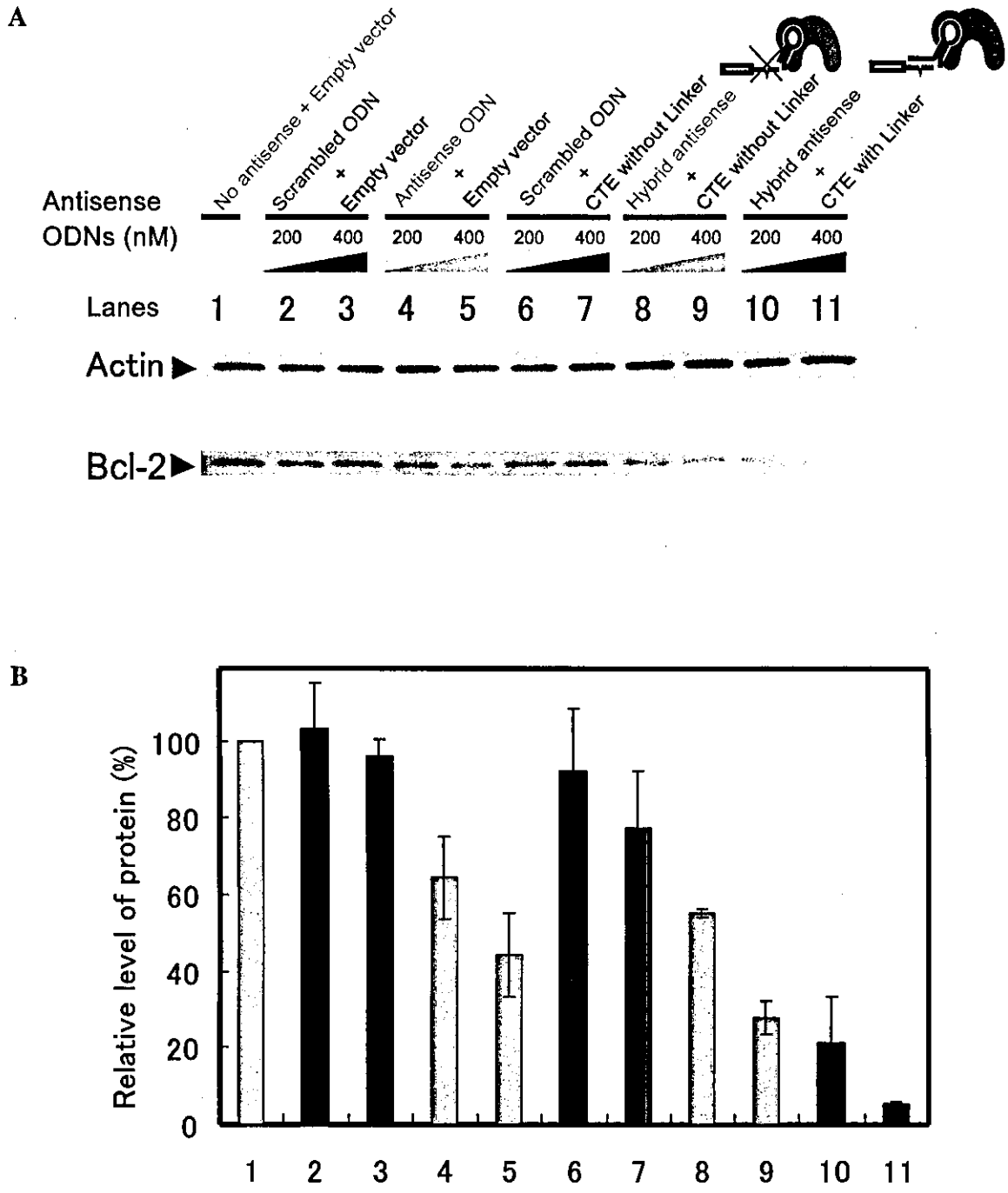


**FIG. 3.** HeLa cells were cotransfected with the CTE-linker expression vector (lanes 10 and 11), the control CTE expression vector (lanes 6–9), or the empty vector (lanes 1–5), together with 200–400 nM *bcl*-2 antisense phosphorothioate ODNs or control ODNs. Twenty-four hours after transfection, cells were harvested and subjected to Western blotting analysis. (A) Western blotting analysis of Bcl-2 and actin. Concentrations of antisense (lanes 4, 5, 8–11) or scrambled (lanes 2, 3, 6, 7) ODNs were 0 nM (lane 1), 200 nM (lanes 2, 4, 6, 8, 10), and 400 nM (lanes 3, 5, 7, 9, 11). (B) The results in A are shown as a histogram. The intensities of bands of immunoreactive actin and Bcl-2 were quantitated using the NIH Image program. Levels of Bcl-2 were normalized by reference to levels of actin. The level in control cells, which were not transfected with antisense ODN, was taken as 100% (column 1). The data are averages from more than three sets of experiments, and error bars are shown.

sense ODNs seemed to be localized in the cytoplasm in the presence of the CTE-linker construct, the observed enhancement of the antisense effects (Fig. 3, lanes 10 and 11) appeared to be reconciled with the findings in Figure 2.

We demonstrated previously that recruitment of RNA helicases significantly enhanced the effects of a ribozyme in cultured cells (Kawasaki et al., 2002; Kawasaki and Taira, 2002a,b; Warashina et al., 2001). In the ribozyme construct, CTE was linked covalently with the ribozyme, and the enhancement achieved as a result of the attachment of the RNA helicase-interacting motif was always significant.

In the hybrid antisense ODN system described in this report, covalent attachment of CTE was not possible, and depending on the target site, the effect was marginal in some cases (data not shown). Nevertheless, we were able to demonstrate clearly that such an approach might be useful, at least against *bcl*-2 as a target. Optimization of the linker sequences should lead to further improvements in this methodology. Furthermore, if we could select a DNA aptamer that would interact with RNA helicases, covalent linkage with the antisense ODN should be possible, which would further improve the system. Although much work remains to be done, we have established a starting point for helicase-recruiting hybrid antisense technology.

## REFERENCES


AL-ALWAN, M.M., ROWDEN, G., LEE, T.D., and WEST, K.A. (2001). Fascin is involved in the antigen-presentation activity of mature dendritic cells. J. Immunol. **166,** 338–345.

BRAUN, I.C., ROHRBACH, E., SCHMITT, C., and IZAURRALDE, E. (1999). TAP binds to the constitutive transport element (CTE) through a novel RNA-binding motif that is sufficient to promote CTE-dependent RNA export from the nucleus. EMBO J. **18,** 1953–1965.

BRAY, M., PRASAD, S., DUBAY, J.W., HUNTER, E., JEANG, K.T., REKOSH, D., and HAMMARSKJOLD, M.L. (1994). A small element from the Mason-Pfizer monkey virus genome makes human immunodeficiency virus type 1 expression and replication Rev-independent. Proc. Natl. Acad. Sci. USA **91,** 1256–1260.

CHU, Z.L., PIO, F., XIE, Z., WELSH, K., KRAJEWSKA, M., KRAJEWSKI, S., GODZIK, A., and REED, J.C. (2001). A novel enhancer of the Apaf1 apoptosome involved in cytochrome c-dependent caspase activation and apoptosis. J. Biol. Chem. **276,** 9239–9245.

COTTER, F.E., WATERS, J., and CUNNINGHAM, D. (1999). Human Bcl-2 antisense therapy for lymphomas. Biochim. Biophys. Acta **1489,** 97–106.

DE LA CRUZ, J., KRESSLER, D., and LINDER, P. (1999). Unwinding RNA in *Saccharomyces cerevisiae*: DEAD-box proteins and related families. Trends Biochem. Sci. **24,** 192–198.

DE SMET, M.D., MEENKEN, C.J., and VAN DEN HORN, G.J. (1999). Fomivirsen—A phosphorothioate oligonucleotide for the treatment of CMV retinitis. Ocul. Immunol. Inflamm. **7,** 189–198.

DEAN, N.M., McKAY, R., CONDON, T.P., and BENNETT, C.F. (1994). Inhibition of protein kinase C-expression in human A549 cells by antisense oligonucleotides inhibits induction of intercellular adhesion molecule 1 (ICAM-1) mRNA by phorbol esters. J. Biol. Chem. **269,** 16416–16424.

DESZO, E.L., BRAKE, D.K., CENGEL, K.A., KELLEY, K.W., and FREUND, G.G. (2001). CD45 negatively regulates monocytic cell differentiation by inhibiting PMA-dependent activation and tyrosine phosphorylation of PKC. J. Biol. Chem. **276,** 10212–10217.

FURDON, P.J., DOMINISKI, Z., and KOLE, R. (1989). RNase H cleavage of RNA hybridized to oligonucleotides containing methyl phosphonate, phosphorothionate and phosphodiester bonds. J. Biol. Chem. **268,** 14514–14522.

GRÜTER, P., TABERNERO, C., VON KOBBE, C., SCHMITT, C., SAAVEDRA, C., BACHI, A., WILM, M., FELBER, B.K., and IZAURRALDE, E. (1998). TAP, the human homolog of Mex67p, mediates CTE-dependent RNA export from the nucleus. Mol. Cell **1,** 649–659.

HÉLÈNE, C., and TOULMÉ, J.J. (1990). Specific regulation of gene expression by antisense, sense and antigene nucleic acids. Biochim. Biophys. Acta **1049,** 99–125.

HO, S.P., BAO, Y., LESHER, T., MALHOTRA, R., MA, L.Y., FLUHARTY, S.J., and SAKAI, R.R. (1998). Mapping of RNA-accessible sites for antisense experiments with oligonucleotide libraries. Nat. Biotechnol. **16,** 59–63.

HODGE, C.A., COLOT, H.V., STAFFORD, P., and COLE, C.N. (1999). Rat8p/Dbp5p is a shuttling transport factor that interacts with Rat7p/Nup159p and Gle1p and suppresses the mRNA export defect of xpo1-1 cells. EMBO J. **18,** 5778–5788.

JANKOWSKY, E., GROSS, C.H., SHUMAN, S., and PYLE, A.M. (2000). The DExH protein NPH-II is a processive and directional motor for unwinding RNA. Nature **403,** 447–451.

KAMESAKI, S., KAMESAKI, H., JORGENSEN, T.J., TANIZAWA, A., POMMIER, Y., and COSSMAN, J. (1993). Bcl-2 protein inhibits etoposide-induced apoptosis through its effects on events subsequent to topoisomerase II-induced DNA strand breaks and their repair. Cancer Res. **53,** 4251–4256.

KANG, Y., and CULLEN, B.R. (1999). The human Tap protein is a nuclear mRNA export factor that contains novel RNA-binding and nucleocytoplasmic transport sequences. Genes Dev. **13,** 1126–1139.

KAWASAKI, H., ECKNER, R., YAO, T.P., TAIRA, K., CHIU, R., LIVINGSTON, D.M., and YOKOYAMA, K.K. (1998). The expression cassette determines the functional activity of ribozymes in mammalian cells by controlling their intracellular localization. Nature **393,** 284–289.

KAWASAKI, H., ONUKI, R., SUYAMA, E., and TAIRA, K. (2002). Identification of genes that function in the TNF-alpha-mediated apoptotic pathway using randomized hybrid ribozyme libraries. Nat. Biotechnol. **20,** 376–380.

KAWASAKI, H., and TAIRA, K. (2002a). Identification of genes by hybrid ribozymes that couple cleavage activity with the unwinding activity of an endogenous RNA helicase. EMBO Rep. **3,** 443–450.

KAWASAKI, H., and TAIRA, K. (2002b). A functional gene discovery in the Fas-mediated pathway to apoptosis by analysis of transiently expressed randomized hybrid-ribozyme libraries. Nucleic Acids Res. **30,** 3609–3614.

KOSEKI, S., TANABE, T., TANI, K., ASANO, S., SHIODA, T., NAGAI, Y., SHIMADA, T., OHKAWA, J., and TAIRA, K. (1999). Factors governing the activity *in vivo* of ribozymes transcribed by RNA polymerase III. J. Virol. **73,** 1868–1877.

KUSHNER, D.M., and SILVERMAN, R.H. (2000). Antisense cancer therapy: The state of the science. Curr. Oncol. Rep. **21,** 23–30.

KUWABARA, T., WARASHINA, M., KOSEKI, S., SANO, M., OHKAWA, J., NAKAYAMA, K., and TAIRA, K. (2001a). Significantly higher activity of a cytoplasmic hammerhead ribozyme than a corresponding nuclear counterpart: Engineered tRNAs with an extended 3′ end can be exported efficiently and specifically to the cytoplasm in mammalian cells. Nucleic Acids Res. **29,** 2780–2788.

KUWABARA, T., WARASHINA, M., NAKAYAMA, A., OHKAWA, J., and TAIRA, K. (1999). $tRNA^{Val}$-heterodimeric maxizymes with high potential as gene-inactivating agents: Simultaneous cleavage at two sites in HIV-1 tat mRNA in cultured cells. Proc. Natl. Acad. Sci. USA **96,** 1886–1891.

KUWABARA, T., WARASHINA, M., ORITA, M., KOSEKI, S., OHKAWA, J., and TAIRA, K. (1998a). Formation of a catalytically active dimer by $tRNA^{Val}$-driven short ribozymes. Nat. Biotechnol. **16,** 961–965.

KUWABARA, T., WARASHINA, M., SANO, M., TANG, H., WONG-STAAL, F., MUNEKATA, E., and TAIRA, K. (2001b). Recognition of engineered tRNAs with an extended 3′ end by exportin-t (Xpo-t) and transport of tRNA-attached ribozymes to the cytoplasm in somatic cells. Biomacromolecules **2,** 1229–1242.

KUWABARA, T., WARASHINA, M., TANABE, T., TANI, K., ASANO, S., and TAIRA, K. (1998b). A novel allosterically *trans*-activated ribozyme, the maxizyme, with exceptional specificity *in vitro* and *in vivo*. Mol. Cell **2,** 617–627.

LAPTEV, A.V., LU, Z., COLIGE, A., and PROCKOP, D.J. (1994). Specific inhibition of expression of a human collagen gene (*COLIAI*) with modified antisense oligonucleotides. The most effective target sites are clustered in double-stranded regions of the predicted secondary structure for the mRNA. Biochemistry **33,** 11033–11039.

LEE, C.G., ZAMORE, P.D., GREEN, M.R., and HURWITZ, J. (1993). Human RNA helicase A is homologous to the maleless protein of *Drosophila*. J. Biol. Chem. **268,** 16822–16830.

LI, J., TANG, H., MULLEN, T.M., WESTBERG, C., REDDY, T.R., ROSE, D.W., and WONG-STAAL, F. (1999). A role for RNA helicase A in post-transcriptional regulation of HIV type 1. Proc. Natl. Acad. Sci. USA **96,** 709–714.

MIYASHITA, T., and REED, J.C. (1993). Bcl-2 oncoprotein blocks chemotherapy-induced apoptosis in a human leukemia cell line. Blood **81,** 151–157.

MONIA, B.P., JOHNSTON, J.F., GEIGER, T., MULLER, M., and FABBRO, D. (1996). Antitumor activity of a phosphorothioate antisense oligodeoxynucleotide targeted against C-raf kinase. Nat. Med. **2,** 668–675.

PATZEL, V., STEIDL, U., KRONENWETT, R., HAAS, R., and SCZAKIEL, G. (1999). Theoretical approach to select effective antisense oligodeoxyribonucleotides at high statistical probability. Nucleic Acids Res. **27,** 4328–4334.

SCHMITT, C., VON KOBBE, C., BACHI, A., PANTE, N., RODRIGUES, J.P., BOSCHERON, C., RIGAUT, G., WILM, M., SERAPHIN, B., CARMO-FONSECA, M., and IZAURRALDE, E. (1999). Dbp5, a DEAD-box protein required for mRNA export, is recruited to the cytoplasmic fibrils of nuclear pore complex via a conserved interaction with CAN/Nup159p. EMBO J. **18,** 4332–4347.

SCZAKIEL, G., HOMANN, M., and RITTNER, K. (1993). Computer-aided search for effective antisense RNA target sequences of the human immunodeficiency virus type 1. Antisense Res. Dev. **3,** 45–52.

TANABE, T., KUWABARA, T., WARASHINA, M., TANI, K., TAIRA, K., and ASANO, S. (2000). Oncogene inactivation in a mouse model—Tissue invasion by leukaemic cells is stalled by loading them with a designer ribozyme. Nature **406,** 473–474.

TANG, H., GAIETTA, G.M., FISCHER, W.H., ELLISMAN, M.H., and WONG-STAAL, F. (1997). A cellular cofactor for the constitutive transport element of type D retrovirus. Science **276,** 1412–1415.

TANG, H., McDONALD, D., MIDDLESWORTH, T., HOPE, T.J., and WONG-STAAL, F. (1999). The carboxyl-terminus of RNA helicase A contains a bidirectional nuclear transport domain. Mol. Cell. Biol. **19,** 3540–3550.

TANG, H., and WONG-STAAL, F. (2000). Specific interaction between RNA helicase A and Tap, two cellular proteins that bind to the constitutive transport element of type D retrovirus. J. Biol. Chem. **275,** 32694–32700.

WAGNER, J.D.O., JANKOWSKY, E., COMPANY, M., PYLE, A.M., and ABELSON, J.N. (1998). The DEAH-box protein PRP22 is an ATPase that mediates ATP-dependent mRNA release from the spliceosome and unwinds RNA duplexes. EMBO J. **17,** 2926–2937.

WALDER, R.Y., and WALDER, J.A. (1988). Role of RNase H in hybrid-arrested translation by antisense oligonucleotides. Proc. Natl. Acad. Sci. USA **85,** 5011–5015.

WALTON, M.I., WHYSONG, D., O'CONNOR, P.M., HOCKENBERY, D., KORSMEYER, S.J., and KOHN, K.W. (1993). Constitutive expression of human *bcl*-2 modulates nitrogen mustard and camptothecin induced apoptosis. Cancer Res. **53,** 1853–1861.

WARASHINA, M., KUWABARA, T., KATO, Y., SANO, M. and TAIRA, K. (2001). RNA-protein hybrid ribozymes that efficiently cleave any mRNA independently of the structure of the target RNA. Proc. Natl. Acad. Sci. USA **98,** 5572–5577.

WESTBERG, C., YANG, J.P., TANG, H., REDDY, T.R., and WONG-STAAL, F. (2000). A novel shuttle protein binds to

RNA helicase A and activates the retroviral constitutive transport element. J. Biol. Chem. **275,** 21396–21401.

ZIEGLER, A., LUEDKE, G.H., FABBRO, D., ALTMANN, K.H., STAHEL, R.A., and ZANGEMEISTER-WITTKE, U. (1997). Induction of apoptosis in small-cell lung cancer cells by an antisense oligodeoxynucleotide targeting the Bcl-2 coding sequence. J. Natl. Cancer Inst. **89,** 1027–1036.

ZOLOTUKHIN, A.S., VALENTIN, A., PAVLAKIS, G.N., and FELBER, B.K. (1994). Continuous propagation of RRE(−) and Rev(−)RRE(−) human immunodeficiency virus type 1 molecular clones containing a *cis*-acting element of simian retrovirus type 1 in human peripheral blood lymphocytes. J. Virol. **68,** 7944–7952.

Address reprint requests to:
*Professor Kazunari Taira*
*Department of Chemistry and Biotechnology*
*School of Engineering*
*The University of Tokyo*
*Hongo, Tokyo 113-8656*
*Japan*

*E-mail:* taira@chembio.t.u-tokyo.ac.jp

Received June 10, 2002; accepted in revised form November 14, 2002.

ANTISENSE AND NUCLEIC ACID DRUG DEVELOPMENT 13:1–7 (2003)


# Comparison of the Suppressive Effects of Antisense Oligonucleotides and siRNAs Directed Against the Same Targets in Mammalian Cells

MAKOTO MIYAGISHI,[1,2] MARIKO HAYASHI,[1] and KAZUNARI TAIRA[1,2]

## ABSTRACT

**RNA interference appears to be a potentially powerful tool for studies of genes of unknown function. However, differences in efficacy at different target sites remain problematic when small interfering RNA (siRNA) is used as an effector. Similar problems are associated with attempts at gene inactivation using antisense oligonucleotides (ODNs) and ribozymes. We performed a comparative analysis of the suppressive effects of three knockdown methods, namely, methods based on RNA interference (RNAi), antisense ODNs, and ribozymes, using a luciferase reporter system. Dose-response experiments revealed that the $IC_{50}$ value for the siRNA was about 100-fold lower than that of the antisense ODN. Our results provide useful information about the positional effects in RNAi, which might help to improve the design of effective siRNAs.**

## INTRODUCTION

THE DRAFT SEQUENCE OF THE HUMAN GENOME (International Human Genome Sequencing Consortium, 2001; Venter et al., 2001) includes many genes of unknown function, and identification of these genes is of great importance. Methods for disrupting the expression of specific genes are critical for accurate analysis of the functions of unknown genes, and at present, three major tools, namely, antisense oligonucleotides (ODNs), ribozymes, and RNA interference (RNAi), are available for suppression of the expression of individual specific genes.

Antisense ODNs are short pieces of synthetic, chemically modified DNA that are designed to bind to their target mRNA via Watson-Crick base pairing, thereby specifically inhibiting the expression of the target mRNA (Dove, 2002). As opposed to the apparently simple theory, the mechanism of inhibition by antisense ODNs seems to involve several complicated steps, including inhibition of translation, splicing, or transport of the target mRNA or degradation of the DNA/RNA hybrid by RNase H.

Ribozymes are RNA molecules with enzymatic activities that bind selectively to and cleave specific target RNAs (Kuwabara et al., 2000a,b; Takagi et al., 2001). It was expected initially that ribozymes might be useful as therapeutic agents and as tools for the functional analysis of genes of interest. However, high-level activities or ribozymes *in vivo* depend on the stability and localization of the transcript, the cleavage activity, and the accessibility of the target RNA to the ribozyme. Nonetheless, a chimeric $tRNA^{Val}$ ribozyme, transcribed at a high level from a pol III promoter, with considerable stability in cells and the capacity for translocation to the cytoplasm, has yielded many successful results in cultured cells and animals (Kato et al., 2001; Koseki et al., 1999; Tanabe et al., 2000).

[1]Department of Chemistry and Biotechnology, School of Engineering, The University of Tokyo, Hongo, Tokyo 113-8656, Japan.

[2]Gene Function Research Laboratory, National Institute of Advanced Industrial Science and Technology (NIAIST), Tsukuba Science City 305-8562, Japan.

RNAi is a recently discovered knockdown phenomenon that is induced by double-stranded RNA (dsRNA) and that has been demonstrated in plants, nematodes, *Drosophila*, protozoa, and mammalian cells (Fire et al., 1998; Fire, 1999; Hammond et al., 2001b; Sharp, 2001; Zamore, 2001; Caplen et al., 2001; Elbashir et al., 2001a). The mechanism of RNAi is not fully understood, but recent genetic and biochemical studies have revealed some details at the molecular level. Inside the cell, dsRNAs are digested into fragments of 21–23 nucleotides (nt), with a 2-nt 3′-overhand, by an RNase III-related enzyme, designated Dicer (Bernstein et al., 2001). Subsequently, these small fragments, known as small interfering RNAs (siRNAs), are incorporated into the RNA-induced silencing complex (RISC) (Hammond et al., 2001a; Nykanen et al., 2001). The active complexes containing the guide RNA recognize and cleave the target RNA.

The activity of siRNA is high even at low concentrations, without apparent toxicity. However, recent reports suggest that the efficacy of siRNA exhibits serious dependence on the target site, as is the case for antisense ODNs and ribozymes, which might significantly limit the convenient use of siRNA (Holen et al., 2002; Miyagishi and Taira, 2002). In the present study, we compared the efficacy of suppression and positional dependency of these knockdown methods, using antisense ODNs and RNAi.

## MATERIALS AND METHODS

*Cell culture, transfections, and assays of expression of reporter genes*

HeLa S3 cells were cultured in Dulbecco's modified Eagle's medium (DMEM) supplemented with 10% fetal bovine serum (FBS). Transfections were performed with Lipofectamine™ 2000 reagent (Life Technologies, Rockville, MD) using 1 nM siRNA or 100 nM ribozymes, as described by the manufacturer. For experiments with antisense ODNs, cells were transfected with 30 ng of an RSV-Renilla luciferase plasmid (pRL-RSV) (Miyagishi et al., 2000), 30 ng of a firefly luciferase expression vector pGL3 (Promega, Madison, WI) using FuGENE 6 (Roche Applied Science, Mannheim, Germany), and 200 nM antisense ODNs using Oligofectamine™

| | | |
|---|---|---|
| Site 1 | siRNA(sense) | 5'-CUUACGCUGAGUACUUCGAUU-3' |
| | siRNA(antisense) | 5'-UCGAAGUACUCAGCGUAAGUU-3' |
| | Antisense ODN | 5'-CATTTCGAAGTACTCAGCGT |
| | Ribozyme | 5'-GGUUGCAACCUGAUGAGGCCGA AAGGCCGAAACUCAGCGUAAG-3' |
| Site 2 | siRNA(sense) | 5'-UUCGUCACAUCUCAUCUACUU-3' |
| | siRNA(antisense) | 5'-GUAGAUGAGAUGAGACGAAUU-3' |
| | Antisense ODN | 5'-GGAGGTAGATGAGATGTGAC |
| | Ribozyme | 5'-GGGGUAGAUCUGAUGAGGCCGA AAGGCCGAAAGAUGUGA-3' |
| Site 3 | siRNA(sense) | 5'-UGCCAGAGUCCUUCGAUAGGG-3' |
| | siRNA(antisense) | 5'-CUAUCGAAGGACUCUGGCACA-3' |
| | Antisense ODN | 5'-CCTATCGAAGGACTCTGGCA-3' |
| | Ribozyme | 5'-GGATCGAAGCTGATGAGGCCGAA AGGCCGAAAACTCTGGC-3' |
| Site 4 | siRNA(sense) | 5'-GUGCGCUGCUGGUGCCAACUU-3' |
| | siRNA(antisense) | 5'-GUUGGCACCAGCAGCGCACUU-3' |
| | Antisense ODN | 5'-TTGGCACCAGCAGCGCACUU-3' |
| Site 5 | siRNA(sense) | 5'-UAAGGAAGUCGGGGAAGCGGU-3' |
| | siRNA(antisense) | 5'-CGCUUCCCCGACUUCCUUAAG-3' |
| | Antisense ODN | 5'-CCGCTTCCCCGACTTCCTTA-3' |
| | Ribozyme | 5'-GGCUUCCCCCUGAUGAGGCCGA AAGCCGAAACUUCCUU-3' |
| Site 6 | siRNA(sense) | 5'-CAGGUGGCUCCCGCUGAAUUG-3' |
| | siRNA(antisense) | 5'-AUUCAGCGGGAGCCACCUGAU-3' |
| | Antisense ODN | 5'-AATTCAGCGGGAGCCAGGTG-3' |
| | Ribozyme | 5'-GGUCAGCGGCUGAUGAGGCCGA AAGGCCGAAAGCCACCU-3' |

**FIG. 1.** Design of siRNAs and antisense ODNs targeted to six sites in the firefly gene for luciferase.

(Life Technologies) in Optimem medium (Life Technologies). Three hours after transfections, the medium was replaced by serum-containing medium. Luciferase activities were analyzed after 24 hours with the dual-luciferase system (Promega).

### *RNA and antisense ODNs*

RNA ODNs were synthesized by an automated synthesizer (model 394) (Applied Biosystems, Foster City, CA). The synthetic RNAs were deprotected and purified by electrophoresis on a denaturing polyacrylamide gel. After elution from the gel, the RNAs were desalted by passage through a NAP-10 column (Amersham Pharmacia Biotech, Piscataway, NJ) in RNase-free water. Fractions were reduced to dryness under a vacuum, and residues were resuspended in annealing buffer (phosphate-buffered saline [PBS], pH 6.8, 2 mM $MgCl_2$). RNA oligonucleotides (10 $\mu$M) were annealed by incubation at 95°C for 1 minute, cooled to 70°C, and subsequent slowly cooled to 4°C for 2 hours. The sequences of the sense and antisense strands of negative control siRNA were follows: sense, 5′-CUU UCA GCU UCG AUG UAG GTT-3′, antisense, 5′-CCU ACA UCG AAG CUG AAA GTT-3′. HPLC-purified phophorothioate ODNs were purchased from Hokkaido System Science Co., Ltd. (Sapporo, Japan). The sequence of the negative control antisense ODN was 5′-CCA ATG TCA AGC ACT TCC GTT-3′. Ribozymes were synthesized from annealed synthetic ODNs by transcription from a T7 promoter using MEGAShortscript™ T7 kit (Ambion, Austin, TX) and purified by electrophotesis on a urea-polyacrylamide gel (7 M urea, 20% polyacrylamide).

## RESULTS

### *Selection of target sites in firefly gene for luciferase*

We used a dual-luciferase assay system to evaluate the suppressive effects of the three knockdown methods, us-

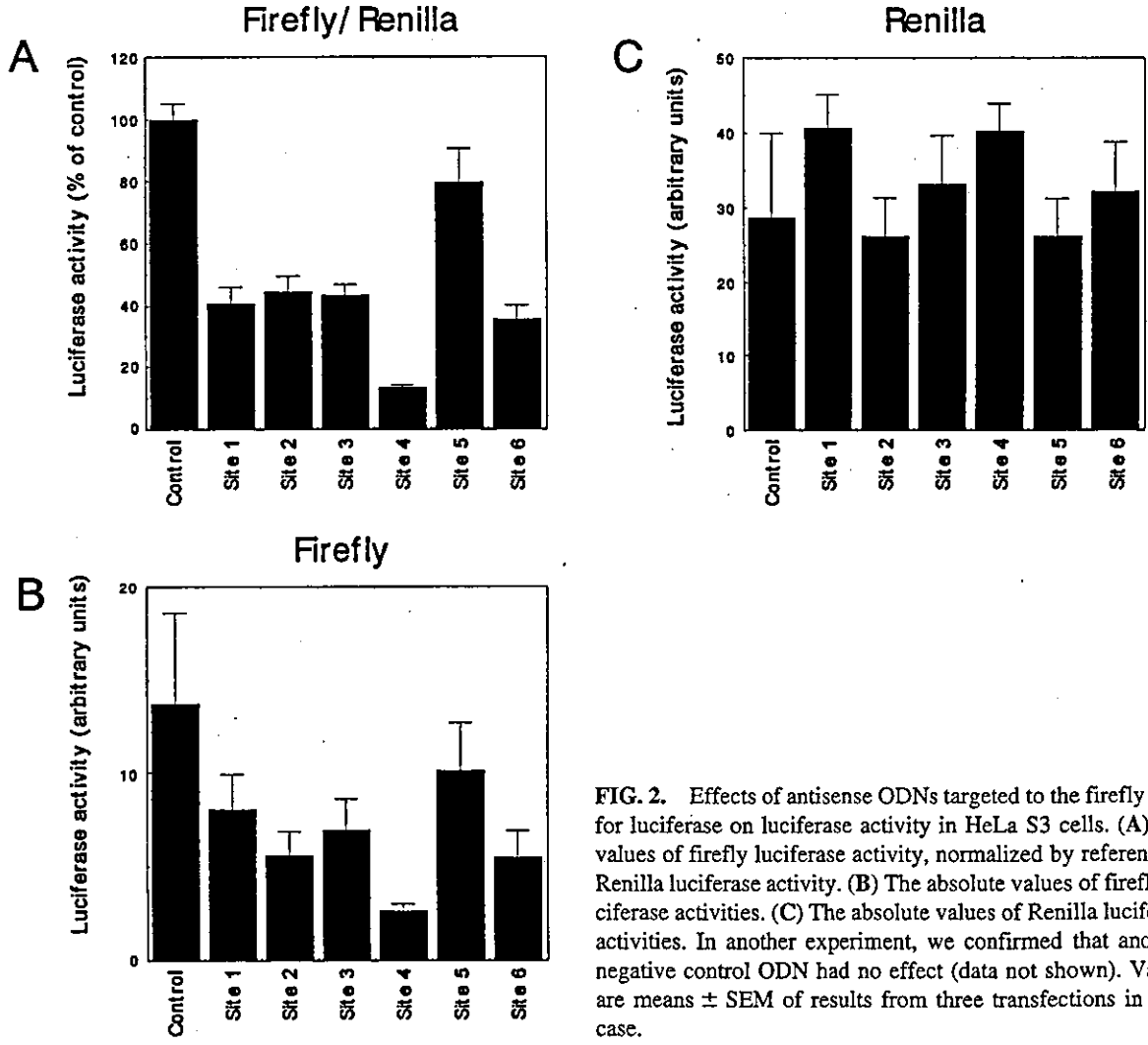


**FIG. 2.** Effects of antisense ODNs targeted to the firefly gene for luciferase on luciferase activity in HeLa S3 cells. (**A**) The values of firefly luciferase activity, normalized by reference to Renilla luciferase activity. (**B**) The absolute values of firefly luciferase activities. (**C**) The absolute values of Renilla luciferase activities. In another experiment, we confirmed that another, negative control ODN had no effect (data not shown). Values are means ± SEM of results from three transfections in each case.